



CRYSTAL GROWTH AND CHARACTERIZATION OF ThO_2 AND $\text{U}_x\text{Th}_{1-x}\text{O}_2$

THESIS

Jacob G. Castilow, Civilian

AFIT-ENP-13-M-06

**DEPARTMENT OF THE AIR FORCE
AIR UNIVERSITY**

AIR FORCE INSTITUTE OF TECHNOLOGY

Wright-Patterson Air Force Base, Ohio

DISTRIBUTION STATEMENT A.
APPROVED FOR PUBLIC RELEASE; DISTRIBUTION UNLIMITED.

The views expressed in this thesis are those of the author and do not reflect the official policy or position of the United States Air Force, Department of Defense, or the United States Government. This work is declared a work of the U.S. Government and is not subject to copyright protection in the United States.

AFIT-ENP-13-M-06

CRYSTAL GROWTH AND CHARACTERIZATION OF ThO_2 AND $\text{U}_x\text{Th}_{1-x}\text{O}_2$

THESIS

Presented to the Faculty

Department of Engineering Physics

Graduate School of Engineering and Management

Air Force Institute of Technology

Air University

Air Education and Training Command

In Partial Fulfillment of the Requirements for the

Degree of Master of Science in Applied Physics

Jacob G. Castilow

Civilian

March 2013

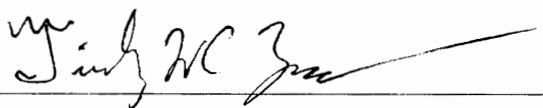
DISTRIBUTION STATEMENT A.
APPROVED FOR PUBLIC RELEASE; DISTRIBUTION UNLIMITED.

CRYSTAL GROWTH AND CHARACTERIZATION OF ThO_2 AND $\text{U}_x\text{Th}_{1-x}\text{O}_2$

Jacob G. Castilow

Civilian

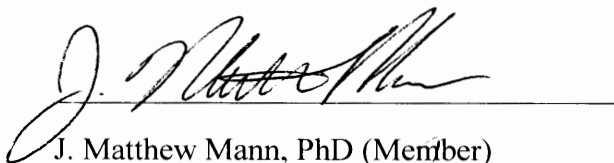
Approved:



Capt. Timothy Zens (Chairman)

04 April 13

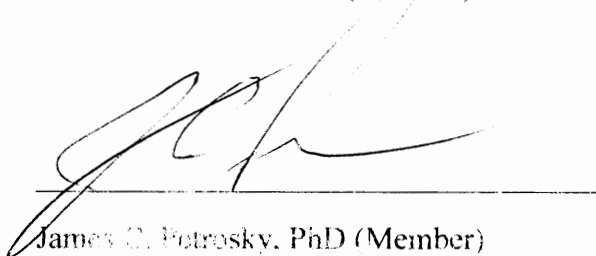
Date



J. Matthew Mann, PhD (Member)

04 April 13

Date



James C. Petrosky, PhD (Member)

04 Apr 13

Date

Table of Contents

Abstract	ix
Acknowledgements	xi
I. Introduction	1
1.1 Thorium as Nuclear Fuel	1
1.2 Comparing Ceramic Fuels to Single Crystal Fuels	4
1.3 Hydrothermal Growth	8
1.4 Previous Research	10
II. Experimental Technique	15
2.1 Hydrothermal Crystal Synthesis in Inert Metal Liners	15
2.1.1 Spontaneous nucleation in 2.5” ampoules	15
2.1.2 Transport runs in 8” ampoules	16
2.1.3 Tuttle Cold Seal Autoclaves	17
2.1.4 Heating System	19
2.2 Structural Characterization	21
2.2.1 Powder X-ray Diffraction	21
2.2.2 Single Crystal X-ray Diffraction	21
2.2.3 Scanning Electron Microscopy and Energy Dispersive X-ray Spectrometry	22
2.2.4 Fluorescence Spectroscopy	22
III. Crystal Growth and Characterization	25
3.1 Lowering the Synthesis Temperature of Bulk ThO ₂	25
3.2 Exploratory Growth of U _x Th _{1-x} O ₂	30

3.3 Bulk Growth of $U_xTh_{1-x}O_2$	36
3.4 Structural and Optical Characterization of Spontaneous Nucleation.....	45
4.1 Future Work	54
4.2 Conclusions	54

List of Figures

Figure 1. The fluorite crystal structure..	3
Figure 2. Thermal conductivity of ThO ₂ as measured by Mann.....	5
Figure 3. Bakker et al. collection of thermal conductivity data for ThO ₂ ceramic powders.	6
Figure 4. Image of single crystals grown by Mann	11
Figure 5. Solubility of thorium dioxide at 750°C.	12
Figure 6. Infrared spectrum of thorium dioxide.....	13
Figure 7. Powder X-ray diffraction of thorium dioxide.....	14
Figure 8. A crystal ladder made from 1mm silver wire.....	17
Figure 9. A representative Tuttle autoclave[27]	19
Figure 10. An assembled Tuttle cold-cone seal autoclave.....	20
Figure 11. Solubility curves for ThO ₂	27
Figure 12. Bulk growth of ThO ₂	28
Figure 13. Comparison of nucleation produced during ThO ₂ bulk growth.	29
Figure 14. Microcrystalline powder obtained from crystal growth in 2.5” silver ampoules	31
Figure 15. EDX spectrum for a reaction with 2% uranium.	32
Figure 17. EDX spectrum for the rod-like crystal structures.....	33
Figure 18. EDX spectrum for a reaction with 50% uranium.	34
Figure 19. An electron micrograph of possible microcrystalline UO ₃	35
Figure 20. EDX spectrum for a reaction containing only UO ₂ and 12M CsF..	35
Figure 21. Bulk growth of U _x Th _{1-x} O ₂ using 12M CsF and a gradient of 685-660°C	38
Figure 22. Bulk growth of U _x Th _{1-x} O ₂ using 12M CsF and a gradient of 685-650°C	39

Figure 23. Nucleation from the reaction containing 40% uranium	40
Figure 24. Elemental mapping of the bulk crystal with 16% uranium concentration	41
Figure 25. Bulk growth of a uranium-thorium alloy from a pre-fabricated feedstock	43
Figure 26. A plot of the lattice parameter against the concentration of thorium	45
Figure 27. Laue pattern for the X-ray diffraction from the (100) plane	47
Figure 28. Rocking curve for the (200) plane in a urania-thoria alloy	47
Figure 29. Photoluminescence spectrum for thorium dioxide.	48
Figure 30. CASINO simulation of ThO ₂	49
Figure 31. CASINO simulation U _{0.04} Th _{0.96} O ₂ . Like the ThO ₂ sample	50
Figure 32. A ThO ₂ spectrum collected using cathodoluminescence spectroscopy.	51
Figure 33. Preliminary CL fit for ThO ₂ data.....	52
Figure 34. U _{0.04} Th _{0.96} O ₂ spectrum collected using cathodoluminescence spectroscopy	53

Abstract

Hydrothermal synthesis of ThO_2 and $\text{U}_x\text{Th}_{1-x}\text{O}_2$, and UO_x at temperatures between 670°C and 700°C has been demonstrated. Synthesis at these temperatures is $50\text{--}80^\circ\text{C}$ below prior crystal growths and represents a new lower bound of successful growth. ThO_2 possesses the highest known melting point of any refractory oxide at $3377\pm 17^\circ\text{C}$. Thus, single crystal synthesis of the refractory oxides ThO_2 , $\text{U}_x\text{Th}_{1-x}\text{O}_2$, and UO_x at these temperatures represents a significant improvement over traditional melt-based crystal growth techniques, which rely on temperatures around 1800°C . Additionally, the impurities from fluxes or melts that have led to poor performance and poor crystal quality are removed. This technique offers a comparatively low temperature and low thermal strain method for crystal growth. Hydrothermal synthesis also represents a cost effective, environmentally friendly way of growing bulk actinide materials of optical quality. These refractory oxide single crystals offer potential applications in thorium nuclear fuel technology, wide-band-gap uranium-based direct-conversion solid state neutron detectors, and understanding how actinide fuels age with time. ThO_2 single crystals of dimensions $6.49\text{mm} \times 4.89\text{mm} \times 3.89\text{mm}$ and weighing 0.633g have been synthesized at growth rates near 0.125mm/wk . Single crystal $\text{U}_x\text{Th}_{1-x}\text{O}_2$ crystals with mole fractions up to $x \approx 0.30$ have also been grown. The largest alloyed crystal with mole fraction $x \approx 0.23$ has dimensions of $2.97\text{mm} \times 3.23\text{mm} \times \sim 3\text{mm}$ and saw growth rates likely near 0.2mm/wk . Mineralizer molarity, temperature gradient, and synthesis temperature were gradually optimized to produce a faceted, cubic crystal approximately 3mm a side.

X-ray diffraction of single crystal ThO_2 determined the unit cell to be of the calcium fluorite structure with a lattice parameter of $5.596(4)\text{\AA}$. Lattice parameters for $\text{U}_x\text{Th}_{1-x}\text{O}_2$ varied linearly with thorium concentration suggesting homogenous uranium incorporation into the lattice. Energy-dispersive spectroscopy (EDS) identified the chemical species as ThO_2 , $\text{U}_x\text{Th}_{1-x}\text{O}_2$, and UO_x without additional impurities within the error of the measurement. Structural studies on the single crystals will enable us to quantify the strain associated with incorporating uranium into the lattice along with measuring the dislocation density as the mole fraction of uranium is increased.

Optically, cathodoluminescence performed at $\sim 25\text{K}$ yielded a signal with multiple shoulders. Preliminary fitting suggests five Gaussians peaks comprise the signal. These broad peaks are consistent with photoluminescence results. Crystal defects, impurities, and inclusions are the likely cause. Photoluminescence has produced an intraband excitation peak at 233 nm and an emission at 350 nm along with an additional peak at 291 nm and an emission at 371 nm for single crystal ThO_2 . Literature suggests a possible europium impurity associated with the 233 nm peak.

Hydrothermal synthesis of bulk actinide materials represents a cost effective method for producing next generation neutron detection materials. Commercially available bulk actinide crystals would open up new possibilities for the detection of weapons of mass destruction, the study of the effect of aging on actinides, and thorium fuel cycle reactors.

Acknowledgements

Foremost, I would like to thank Capt. Timothy Zens for his guidance and for providing me with the resources necessary to be successful in this endeavor. Further, I'd like to thank Dr. Matthew Mann for providing insight into the hydrothermal growth technique and freely offering advice on growth conditions. Dr. Petrosky was also of help offering advice on motivations behind the research and suggesting characterization experiments to be performed. I also appreciate Dr. Kolis providing the space and equipment necessary for crystal growth. He was ever encouraging about experimental results. I'd especially like to thank Dr. Colin McMillen for his expert opinion "in the trenches". Dr. McMillen has a seemingly infinite amount of patience for questions and mistakes. In all things crystal-related, he was a wonderful tutor. I'd also like to thank the other members of the Kolis research group for their advice and help in crystal growth and characterization. Lastly, thanks to the many people including Dr. Giles, Dr. Adam Brandt, Dr. Kiefer, Maj. Mike Lee, Wally Rice, and Greg Smith who assisted in data collection.

Twelfth-century philosopher Bernard of Chartres is attributed with saying: "We are like dwarfs on the shoulders of giants, so that we can see more than they, and things at a greater distance, not by virtue of any sharpness of sight on our part, or any physical distinction, but because we are carried high and raised up by their giant size." More than eight hundred years has passed since this attribution, yet the sentiment remains the same today. The body of work presented herein would not have been possible without the generous help of many giants.

I. Introduction

1.1 Thorium as Nuclear Fuel

The quest for a clean energy source is ongoing. However, the one technology that already exists, produces useable quantities of energy, and has comparable emissions of carbon dioxide to renewable sources is nuclear energy[1].

The controversy surrounding nuclear power is familiar to many people. Opponents of the current uranium based fuel cycle contend that nuclear power poses numerous threats to humans and the environment. Possible threats include problems with processing, transporting, and storage of nuclear waste, the danger associated with nuclear weapons proliferation and terrorism, along with general health risks and environmental damage due to uranium mining[1].

The International Atomic Energy Agency has been publishing reviews based on conference presentations since the mid-nineties on the benefits and challenges of using a thorium-based fuel cycle. These reviews comprehensively lay out the benefits of a nuclear fuel cycle based on thorium. The benefits of using a thorium-based nuclear fuel listed below are a summary of information presented in IAEA-TECDOC-1450 unless cited otherwise[2]. In terms of natural abundance thorium is three to four times more abundant than uranium, and thorium is distributed across many countries. Moreover, nearly one-hundred percent of thorium extracted can be used; whereas, only seven tenths of a percent of mined uranium is useful as a nuclear fuel.

Virtually all of naturally occurring thorium is ^{232}Th . This isotope is not fissile, but it is fertile – meaning it can be converted to fissile ^{233}U through neutron capture. The pertinent nuclear reaction is the transmutation of ^{232}Th to ^{233}Th through neutron irradiation, then ^{233}Th undergoes two subsequent beta decays, emitting an electron and an anti-neutrino, to become fissile ^{233}U . ^{232}Th absorption cross-section for thermal neutrons (7.4 barns) is almost three times that of ^{238}U (2.7 barns) making thorium a more ‘fertile’ material than uranium for thermal reactors. Additionally, the fissile uranium produced from thorium transmutation can be used for breeding in the thermal neutron spectrum. The difference in decay chains between thorium and uranium also has consequences for the radioactive waste produced in the fuel cycle. Thorium oxide’s fission product release rate is one order of magnitude lower than that of uranium oxide, thus the thorium fuel cycle produces a much smaller quantity of plutonium and long-lived minor actinides.

Chemically, thorium dioxide is more stable and is a more radiation hardened material than uranium dioxide. The greater chemical stability of thorium oxide compared to uranium oxides owes to thorium oxide only existing in the fluorite structure, which is partly due to thorium only being stable in the 4+ oxidation state[3]. The fluorite structure is shown in Figure 1. Whereas, comparatively, uranium possesses multiple oxidation states and can form a wide variety of compounds ranging from UO to U_3O_8 . This may lead to unwanted side reactions *in situ* and during storage of waste products. Another positive benefit of the fluorite structure is its ability to incorporate dopants[4]. This becomes especially important because thorium fuels need a fissile dopant to begin converting the fertile ^{232}Th into fissile ^{233}U .

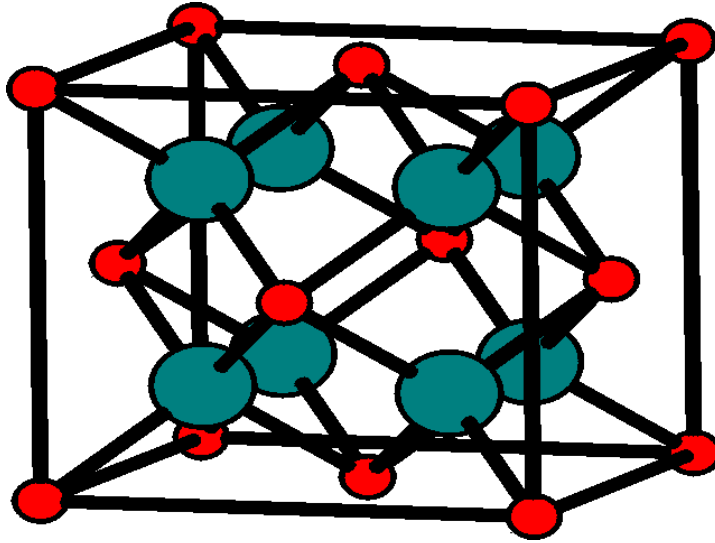


Figure 1. The fluorite crystal structure. Thorium atoms are shown in red, while oxygen atoms are blue. The Th cation sublattice is FCC, while the oxygen atoms occupy all the tetrahedral sites. Hence, there are 4 Th atoms and 8 O atoms per unit cell. Empirically, the fluorite structure is known for incorporating a wide range of dopants; zirconia is a prime example of the wide range of dopants a fluorite structure can tolerate.

The thermophysical properties of thorium are better suited for nuclear fuel use than those of uranium. Thorium's higher thermal conductivity and lower coefficient of thermal expansion as compared to uranium oxide suggest better performance as a nuclear fuel. Higher thermal conductivity values would serve to enhance heat removal thus keeping fuel center temperatures lower, which in turn reduce fission product migration and fuel swelling. Decreased values of thermal expansion prevent detrimental fuel-cladding interaction and reduce swelling[5]. Chaplot et al state, "Nuclear reactor performance is mainly restricted by thermal expansion and thermal conductivity of the fuel pellets under irradiation conditions[5]." The chemical stability of thorium dioxide allows it to resist oxidation and plays a critical role in interim and long-term storage prospects. In contrast, UO_2 easily oxidizes to U_3O_8 and UO_3 which increases the complexity of evaluating and designing safe long-term storage solutions because the different chemistry of each species must be taken into account.

Most importantly, thorium dioxide fuels offer better resistance to weaponization given that the uranium produced through transmutation in the thorium fuel cycle cannot be used in nuclear warheads. Furthermore, weapons-grade plutonium can be disposed of using thorium-plutonium fuels since plutonium is not bred in the reaction and the end product is the same uranium produced in transmutation of thorium.

1.2 Comparing Ceramic Fuels to Single Crystal Fuels

Currently, ThO_2 -based mixed oxide fuels made of doped, pressed ceramics dominate commercial fuels. While easy to fabricate, these possess a number of severe flaws. Foremost, due in part to variation in uranium particle morphology and size, reported thermal conductivity values are inconsistent with values ranging from 9 to $15\text{Wm}^{-1}\text{K}^{-1}$ at 300K[6][7].

Ceramic fuels also suffer from corrosion issues. Pressed ceramics contain many surface defects thus promoting disassociation of water[8]. This disassociation along with conditions in the reaction chamber can lead to formation of hydrogen gas[9]. The expansion of the hydrogen gas under heating can crack the fuel rod and expedite corrosion of the fuel rod. If the fuel rod becomes cracked, the formation of higher oxides of uranium becomes likely leading to volume changes, which can break the cladding.

Single crystals address many of these issues, as they have limited porosity and lower surface defect concentrations decreasing the chance of corrosion of the fuel. Additionally, the thermal properties, which are a key determinant of reactor performance, are much more consistent and often better for single crystals than those of pressed ceramics. We can compare the published results of Mann[10] against the literature values cited above. Results from each source are shown in Figure 1 and Figure 2, respectively.

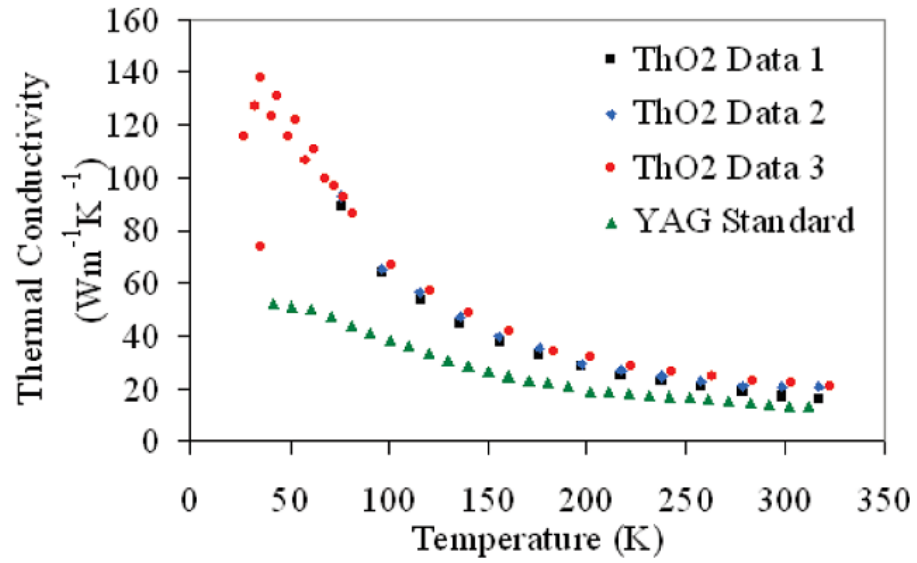


Figure 2. Thermal conductivity of ThO₂ as measured by Mann. The thermal conductivity at 300K is 18-20 WmK. The sample had a density of 96.7% the theoretical value, though no corrections were made for the non-ideal density. Higher thermal conductivity leads to better heat flow through the fuel rod. Keeping the fuel rod cooler lessens thermal expansion and the likelihood of breaking the fuel cladding[10].

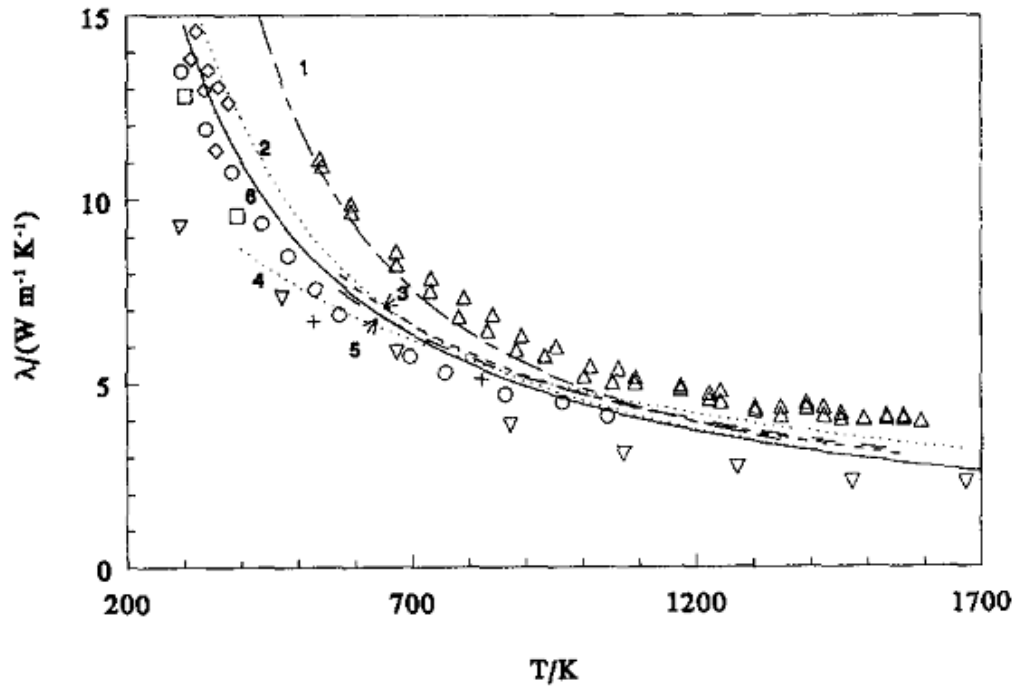


Figure 3. Bakker et al. collection of thermal conductivity data for ThO_2 ceramic powders. At 300K, the thermal conductivity varies between 9 to $15\text{Wm}^{-1}\text{K}^{-1}$. This data represents the highest quality samples with the most consistent data. This data also has been corrected for a density of 95% of the theoretical value. We see that the spread of the thermal conductivity data is three times greater than for single crystal ThO_2 suggesting single crystals may perform more consistently than pressed ceramic powders.

These data strongly make the case for single crystals over pressed ceramics. The data sets shown in Figure 2 were selectively chosen and represent the best case for thorium mixed-oxide ceramics; Bakker et al. rejected ten other data sets choosing the data from the highest quality samples and with the highest quality data. The data were corrected to 95% theoretical density, too. Still, the values range from 9 to $15\text{Wm}^{-1}\text{K}^{-1}$ at 300K. In comparison, Mann's single crystal sample had thermal conductivity values ranging from $18\text{-}20\text{Wm}^{-1}\text{K}^{-1}$. Mann also checked the density of his sample with a helium gas pycnometer and found his sample to be 96.7% of the theoretical density but did not make corrections for the less-than-ideal density. Further, the single crystal under investigation was cloudy and had a small crack. These microscopic and

macroscopic defects contribute to a lower density and overall lower thermal conductivity measurement. An increase in crystal quality is expected to produce an increase in the thermal properties. When comparing the spread in the data at 300K, we see single crystals have one-third of the spread of pressed ceramics. This fact suggests more consistent thermal performance from single crystals. Lastly, hydrothermal growth of ThO₂ single crystals circumvents the high sintering temperatures necessary to reach sufficient density in pressed pellets, which are generally two-thirds of the melting temperature.

The difficulty of fabricating single crystals versus pressed ceramics may explain the lack of research or interest in single crystal thorium oxide. Thorium dioxide, commonly referred to as thoria, is a refractory oxide. The melting point of thoria has been established as $3377 \pm 17^\circ\text{C}$, the highest known for any oxide species[11]. The melting point of thoria precludes the use of traditional melt based techniques like Czochralski growth. While more exotic melt based techniques like skull melting and solar furnaces have been developed nearly all suffer from glaring defects such as striations[12], oxygen deficiencies[13], and poor size and quality in general[14].

The intractability of melt based techniques for growing thoria single crystals has led to extensive research in flux growth techniques[15][16][17][18]. Flux based techniques suffer from flux inclusions. To date, lead-based fluxes have proven most useful in synthesis ThO₂, however the crystals develop color centers from lead flux inclusions[15][19]. Impurities in single crystals of thoria would possibly inhibit the physical and chemical properties which make thorium dioxide beneficial as a nuclear fuel. Moreover, flux inclusions could possibly undergo unwanted nuclear reactions in the reaction chamber leading to further problems.

1.3 Hydrothermal Growth

Laudise and Ballman define hydrothermal synthesis as: “the use of aqueous solvents under high temperature and high pressure to dissolve and recrystallize materials that are relatively insoluble under ordinary conditions[20].” The growth of large bulk crystals occurs beyond the critical point of water (374°C, 3204psi), which is important because supercritical water has excellent dissolving and diffusion properties. Supercritical water can effuse into a solid like a gas while dissolving materials like a liquid[21]. Additionally, diffusion of supercritical fluids is often faster than liquids[22]. Both dissolution and diffusion are integral components of successful hydrothermal growth. To assist in dissolution of the feedstock, a mineralizer is often added to the solution. Mineralizers typically include hydroxide, fluoride, chloride, or carbonate ions. The basic premise of hydrothermal growth is to dissolve feedstock in a “relatively” hot region and through convective transport to a “relatively” cool region deposit the feedstock on either a seed crystal (bulk transport growth) or have the feedstock spontaneously crystallize (spontaneous nucleation).

Looking in more detail at spontaneous nucleation is useful for understanding why nucleation happens and why a mineralizer is necessary. Nucleation is a trade-off between surface energy and the undercooling of a solution. Undercooling is the difference between the melting temperature and the temperature of the solution. For low temperature solutions, particles would prefer to solidify because the surface energy is less than the energy of remaining in solution. As an example let us look at UO_2 , which is somewhat similar structurally to ThO_2 . For UO_2 in a 700°C solution, the radius at which nucleation forms is 0.889\AA , which is less than the U-O bond length meaning all nuclei will grow – neither U nor O want to be in solution at all and will readily bond with each other to form a solid. The critical radius at which a solid forms will be

even less for ThO_2 because Th is larger than U and ThO_2 's melting temperature is nearly 1000°C higher. Thus, lowering the energy of being in solution is necessary for dissolution and transport of feedstock. This is accomplished in two ways: the use of a mineralizer to complex with the feedstock and the use of supercritical water, which has enhanced solubility over ordinary water[23].

Advantages of hydrothermal growth include the “relatively” low temperatures of crystallization, which makes the method an ideal candidate to synthesize refractory oxides[20]. The temperatures rarely exceed 750°C , which is far lower than temperatures usually associated with melt reactions - often greater than 1800°C [24]. This drastic reduction in temperature should lead to a reduction in the point defect concentration by multiple orders of magnitude[25]. Another benefit is the general isothermal bath the crystals are grown in[24]. The seed crystals remain in a bath of mineralizer solution at the same temperature throughout the entire growth run. The low temperature of crystallization and the isothermal growing conditions lead to very high quality crystals with minimal thermal strain, minimal defects[24], and uniform growth and doping. Lastly, the closed atmosphere provided by the sealed growth vessel minimizes impurities while allowing for stabilized reaction conditions[24].

Key to successful hydrothermal growth is the reliability of the reaction vessel. Due to the high temperatures and pressures associated with the growth an autoclave must be used. The autoclave must be reliable and easily sealed, easily assembled and disassembled, and possess high strength characteristics[20]. In this study, we will use autoclaves made of Inconel 718 and employ a Tuttle cold seal as the sealing mechanism. This sealing mechanism is self-energizing and can be reasonably expected to withstand pressures of 2400 atmospheres and temperatures of 750°C [20]. To address the caustic mineralizer solution that is used to dissolve the feedstock, an

inert metal liner such as silver, platinum, or gold maybe be used inside the autoclave. In our case silver turns out to be sufficient to resist corrosion and the most cost effective. Finally, two band heaters will be used to create the thermal gradient that transports the feedstock between the solubility zones inside the autoclave.

1.4 Previous Research

To date only Mann has successfully grown thoria single crystals of good quality and size using the hydrothermal growth technique[10]. As such, we will rely almost exclusive on his previous work for our research. However, Mann synthesized ThO_2 at temperatures near 750°C , while we grew ThO_2 at temperatures near 670°C due to the advantages previously discussed. A sample single crystal from Mann's work is shown in Figure 3 below. The crystals shown in Figure 3(a) represent the results of spontaneous nucleation runs, which are characterized by many small crystals. In contrast, the crystal in Figure 3(b) is the result of seeded transport growth, which is characterized by a single, larger crystal. The crystal of Figure 3(b) is nearly twice as large as those in Figure 3(a).

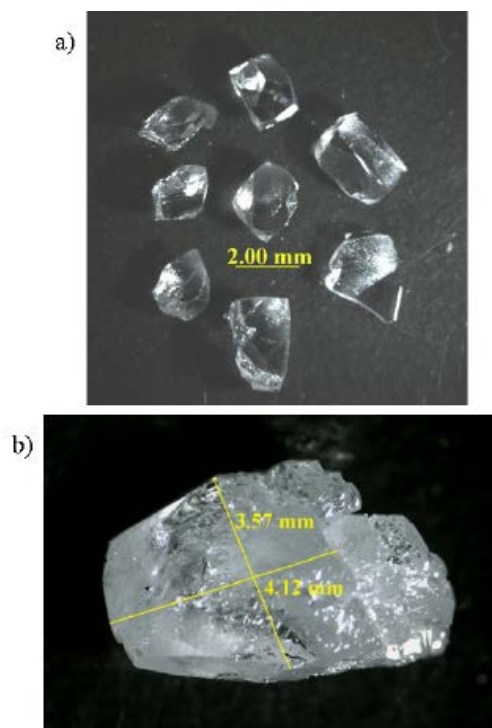


Figure 4. Image of single crystals grown by Matthew Mann. The crystals shown in (a) are the result of spontaneous nucleation events, whereas the crystal shown in (b) was grown using the nucleatation crystals as seeds in a bulk transport growth. Spontaneous nucleation reactions are grown in smaller vessels and conditions are less tightly bound. The goal is to have small crystals form with only feedstock present and no seed. Hence, the difference in crystal size.

Critical to the hydrothermal growth of thorium single crystals are solubility studies and assessments of contaminants due to the mineralizer solution or feedstock impurities. Mann's results are congruent with the high quality growth expected from hydrothermal synthesis. At 750°C thorium dioxide was found to have increasing solubility in cesium fluoride up to approximately 15M. The results of the solubility study are shown in Figure 4. A benchmark of 1% weight percent solubility is considered the minimum needed for acceptable growth rates. However, a tradeoff exists at higher molarity values between quality of growth and growth rates.

Higher values of molarity can also be used to compensate for lower synthesis temperatures, but the gradient between zones may need adjusted to avoid excessive supersaturation.

Additionally, the single crystals were found to be free of fluoride and hydroxyl inclusions. Energy dispersive X-ray analysis was performed to check for fluoride substitutions and none were found. Addressing the possibility of hydroxyl ion inclusion, infrared spectroscopy was performed to check for the broad 3400cm^{-1} stretch associated with a hydroxyl group. The spectrum is shown in Figure 5. The characteristic stretch was absent from the spectrum.

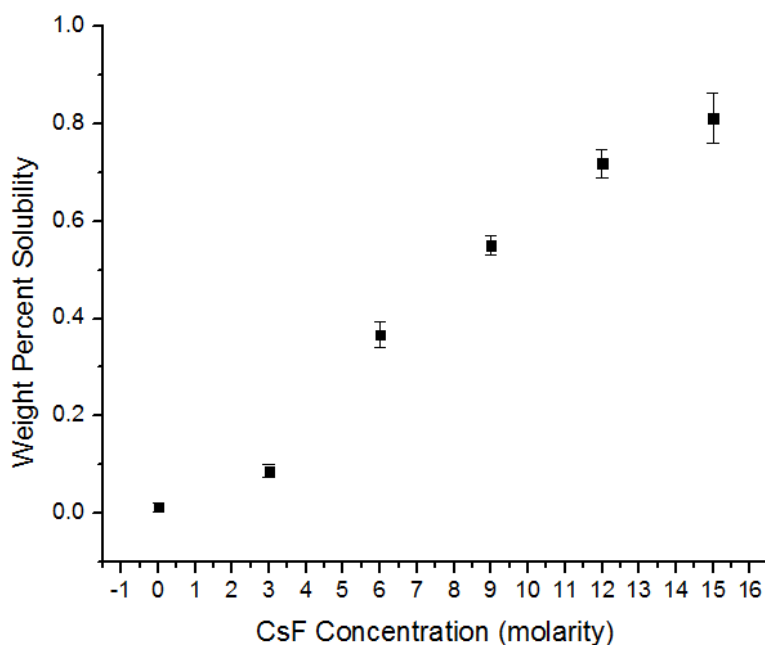


Figure 5. Solubility of thorium dioxide at 750°C measured as weight percent of feedstock dissolved increases up to 15M in cesium fluoride. The curve begins leveling off at 15M. A weight percent value of 1% is considered the benchmark needed to obtain acceptable growth rates. Approximately 0.8% weight percent value was obtained at 15M.

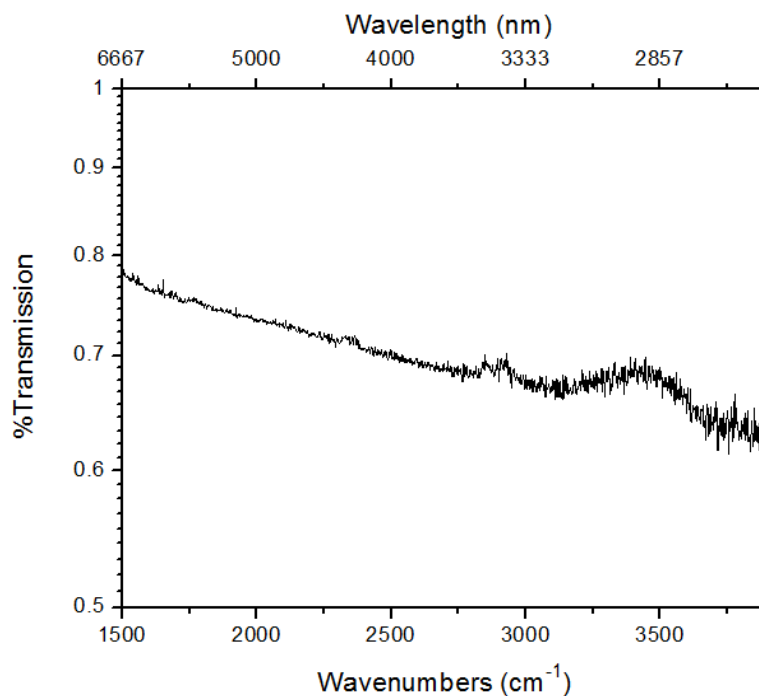


Figure 6. Infrared spectrum of thorium dioxide. A common problem of hydrothermal growth reactions is the inclusion of hydroxyl species in the single crystal. The hydroxyl species has a very distinct broad stretch at 3400cm⁻¹. This stretch is absent in the spectrum shown above indicating that the hydroxide ion is not incorporating in the thoria single crystal.

As a preliminary investigation of crystal quality Mann has performed XRD on his single crystals. The results along with the powder diffraction file (PDF) for thorium dioxide are shown below in Figure 6.

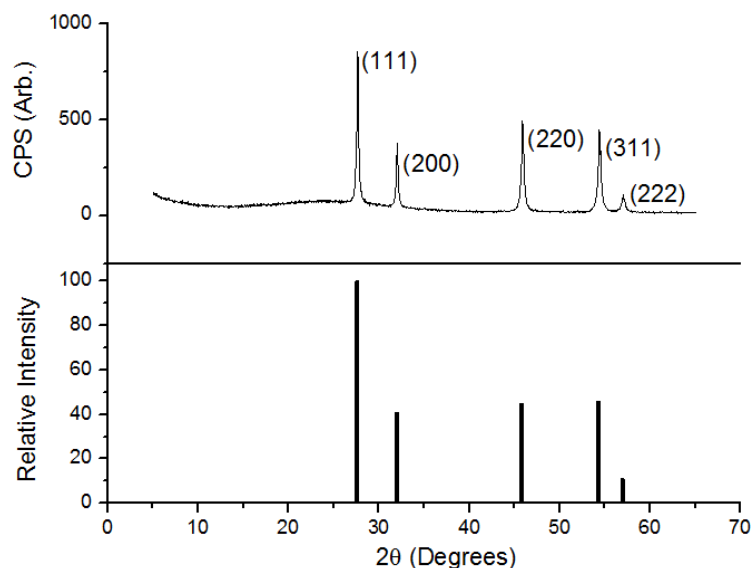


Figure 7. Powder X-ray diffraction of thorium dioxide. The positions and relative intensities of the peak match the reference powder diffraction file for thorium dioxide. Agreement between the peak positions is an indication of chemical identity and crystal quality, and matching relative intensities provides information on the crystal phase and suggests adequate sample preparation. The PDF card number for ThO_2 is 42-1462.

The X-ray diffraction spectrum of the thorium dioxide single crystal agrees with the reference file for thorium dioxide. Both the positions and relative intensities are in agreement. The peak locations differ from the PDF file by at most 0.08° and relative intensities differ by 6% on average from the reference file. Matching both the peak location and relative intensity is a good indication of chemical identity, crystal phase, adequate sample preparation, crystallite size, and residual stress[26].

II. Experimental Technique

2.1 Hydrothermal Crystal Synthesis in Inert Metal Liners

In hydrothermal synthesis, the use of corrosive mineralizers necessitates the use of inert metal liners or ampoules inside the autoclave. In this study, silver (99.9%) ampoules were used because of silver's inertness to highly alkaline mineralizer solutions, specifically the fluoride anion acting as a strong Lewis base, and its relatively low cost compared to other inert metal liners – gold and platinum. The ampoules vary in outer diameter size and length based on the reaction. The silver ampoules are welded shut using a CEA model TOP-165HF inert welder using a carbon electrode under argon flow. Welding the ampoules shut ensures a closed reaction environment. Welding also prevents any corrosive chemicals from leaking out of the ampoule and damaging the inner walls of the autoclave.

2.1.1 Spontaneous nucleation in 2.5" ampoules

Studies geared toward exploratory chemistry took place in silver ampoules with outer diameters of 1/4" and lengths of 2.5". After welding one end of the ampoule shut, powdered feedstock weighing approximately 0.200g was added to ampoule. Reactants for this particular study included powdered ThO_2 and UO_2 synthesized from the decomposition of uranium acetate. The mineralizer solution was prepared then inserted into the ampoule using a syringe. For spontaneous nucleation studies, 0.4 mL of CsF mineralizer was added. CsF had previously proved to be the mineralizer with the highest wt% solubility of ThO_2 . Once all the reactants had been added to the ampoule, the open end was crimped shut with pliers and then welded. Five

sealed ampoules will fit simultaneously inside the autoclave. These reactions yield microcrystalline powders, see Figure 18.

Spontaneous nucleation performed in silver ampoules with outer diameters of 3/8" and lengths of 8" is an exception to performing spontaneous nucleation in 2.5" ampoules. The increase in ampoule size leads to larger, spontaneously nucleated crystals. The purpose of these growth runs is to produce single crystals to be used as seeds and nutrient feedstock to be used in bulk crystal growth. To promote crystallization from solution without a seed, a large gradient, often near 100°C, is applied.

2.1.2 Transport runs in 8" ampoules

Once exploratory growth runs have been optimized to produce the desired products, the reactions are scaled up to produce macroscopic crystals. These crystal growth experiments are called transport runs because feedstock is transported through convective flow to a seed crystal. Transport runs are performed in silver ampoules with outer diameters of 3/8" and lengths of 8" and require preparing a seed and making a growth ladder. The bottom end of the silver tube is still crimped and welded before feedstock and mineralizer are added. In this study, nutrient feedstock amounts and mineralizer solution volume were increased ten-fold from the spontaneous nucleation experiments. Approximately 2.00g of nutrient feedstock was added to the ampoule followed by the addition of 4mL of mineralizer via syringe.

Seeds for transports runs need to be approximately 3mm in size. A hole of 0.75mm is drilled in the center of the crystals. Next, a growth ladder needs to be prepared. The ladder functions as a secure place to hang the seeds, which ensures a uniform temperature bath for the duration of the growth experiment. Ladders are made by using 1mm silver wire (Alfra Aesar,

99.9%) to construct the rails while small sections of 1/4" silver tubing crimped onto the wire rails are used to make rungs. The seed is secured to 0.1mm silver wire (Alfa Aesar, 99.997%). The silver wire is then knotted to two rungs of the crystal ladder, and the ladder and seed structure is ready for use. Several seeds can be hung on a single ladder to explore crystal growth at different temperatures in a single run. Hanging multiple seeds is also a way to increase the amount of material produced from a crystal growth experiment. An example of a crystal ladder with seed suspended is shown in Figure 7.



Figure 8. A crystal ladder made from 1mm silver wire using 1/4" silver tubing as rungs. The seed crystal is suspended from 0.1mm silver wire that has been tied between two rungs. Using several seeds on a single ladder can be a way to explore synthesis at different temperatures.

The ladder is inserted into the silver ampoule. The top is crimped and welded shut. The last remaining step in preparing the ampoule is to slightly compress the middle section of the ampoule between the feedstock and the seed. Further crushing of the ampoule from counter pressure during the reaction will happen along this already deformed section[1].

2.1.3 Tuttle Cold Seal Autoclaves

With the ampoules sealed, they are ready to be placed in an autoclave. This study employs the use of Tuttle cold seal autoclaves. The autoclaves are built out of a nickel-based superalloy, Inconel 718. Thus, the autoclaves can tolerate temperatures of 800°C and pressures far beyond those generated in this study[19]. Byrappa states the Tuttle cold-cone seal can withstand pressures of 5kbar or roughly 72,500PSI[23]. Pressures encountered during the growth

of ThO_2 were approximately 15,000PSI, thus far below the expected limit. The internal volume of the Tuttle autoclave is 27mL with a 0.5” bore. This volume is enough to hold five 2.5” silver ampoules or two 8” ampoules.

Once the silver ampoules have been placed in the autoclave, water is added to the remaining volume of the autoclave until it was approximately 1cm from the lip. The water acts as a counter pressure. The counter pressure keeps the ampoules from bursting during heating. The autoclave now needs to be sealed. Sealing the autoclave is accomplished by threading a cap nut containing a conical plunger onto the top of the autoclave. Before threading the cap nut onto the autoclave, it is important to clean the threads using a bench grinder then apply a copper based grease to the threads. This prevents the cap nut from seizing onto the autoclave at high temperatures. The cap nut forces the 59° conical lip of the plunger against the 60° conical lip of the autoclave, creating a line seal[23]. Additional equipment including high pressure tubing, pressure relief valve, and a pressure gauge are attached to the cap nut. The gauge allows continuous monitoring of the pressure inside the autoclave. The pressure relief valve is used to vent reactions that been overfilled, either intentionally or unintentionally. One would intentionally overfill a reaction to reach a specific desired pressure. This is done by overshooting the desired pressure then venting in small amounts until the autoclave is at the desired pressure. A burst disc may also be added into this plumbing as an additional safety feature. The plunger has a small hole bored down the middle, which allows excess water vapor to be let off and internal pressure monitored. A schematic of a Tuttle autoclave is shown in Figure 8.

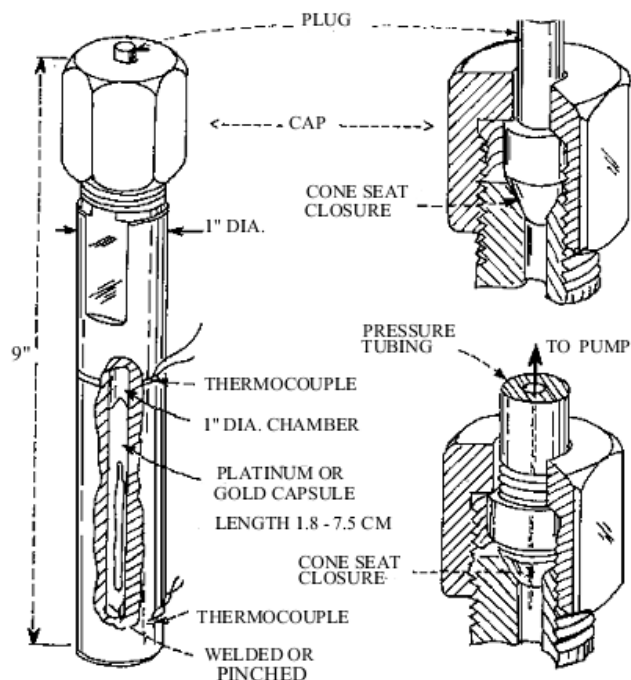


Figure 9. A representative Tuttle autoclave[27]. This schematic demonstrates the inner workings of the Tuttle autoclave. A schematic of the sealing mechanism is shown on the right. The cap nut forces the 59° conical lip of the plunger against the 60° conical lip of the autoclave, creating a line seal. On the left, the position of an inert metal capsule/ampoule inside the autoclave is also shown.

An assembled autoclave used in this study is shown in Figure 9.

2.1.4 Heating System

Hydrothermal synthesis of bulk single crystal material relies on creating a zone where solubility is favored and another zone where crystallization is favored. This is done through the use of differing temperatures on the top and bottom of the autoclave. The different temperatures zones also generate convective flow of the mineralizer solution. This works to dissolve the nutrient feedstock and transport it to the cooler region with the seed. The heating system used consisted of two Mor Electric (N-76580) band heaters. These band heaters provide access to

temperatures near 750°C while also allowing a high degree of zonal temperature control.

Specifically, the arrangement of band heaters plays a key role in determining the temperature profile inside the autoclave. An example of this can be seen in the commercial production of quartz where many, small (2.54cm) band heaters are employed to create isothermal zones. The use of many small band heaters often leads to a more regulated temperature than two large band heaters. Hydrothermal laboratories often measure the temperature profile inside an autoclave for a given arrangement of band heaters, however this data is generally not published.



Figure 10. An assembled Tuttle cold-cone seal autoclave used in this study. The autoclave consists of an Inconel 718 chamber and cap nut, high pressure tubing, pressure relief valve, and pressure gauge. The pressure relief valve is used to vent reactions that have been overfilled, either intentionally or unintentionally.

The band heaters are clamped to the autoclave, and then the autoclave is lowered into a cinder block pit. The pit is filled with vermiculite insulation. This serves to absorb the generous

amounts of heat given off while also acting as a safety feature in the case of an autoclave rupturing. Depending on the goal of the synthesis the autoclave stayed in the pit between 10 and 45 days. Spontaneous nucleation reactions in 2.5” ampoules were given around 10 days; large-scale spontaneous nucleation reactions in 8” ampoules were given around 20 days; and seeded transports runs in 8” ampoules were given around 45 days.

2.2 Structural Characterization

2.2.1 Powder X-ray Diffraction

Microcrystalline powder from spontaneous nucleation or single crystals finely ground could be identified using powder X-ray diffraction. The powder is placed on a zero background sample holder. Reflection patterns were obtained using a Scintag XDS 2000 diffractometer employing Cu K α ($\lambda = 1.54056\text{\AA}$) X-rays. Sample data was collected in step scan mode with a 0.03° step size over a 2θ range of $5-65^\circ$. X-rays were applied at each step between 0.5-5 seconds per step. The diffractometer and data processing was controlled by the DMNST software program. The program’s search match feature was used for identification by comparing experimental peaks with index reflection patterns in the ICDD diffraction database.

2.2.2 Single Crystal X-ray Diffraction

Single crystal X-ray diffraction (SXRD) allows for determination of chemical identity and crystal quality. Crystals with sizes around 0.10-0.25mm are best suited to the particular diffractometer used in this study. Crystals of these sizes are often found among the polycrystalline powder from crystal synthesis in 2.5” silver ampoules. The crystals are mounted on the end of a glass fiber using epoxy. The diffractometer, a Rigaku AFC8 diffractometer

employs the Mo K_{α} ($\lambda=0.71073$) to probe the sample with X-rays. Reflections are captured on a Mercury CCD area detector. Data collection, processing, and integration are controlled using the Crystal Clear software package. Preliminary determination of crystal phase and lattice parameter was done by collecting four images with ω at 0, 30, 60, 90°, while keeping χ and Φ fixed at 0°. The reflections were compared to known unit cells in the Inorganic Crystal Structure Database (ICSD). Agreement between lattice parameters and crystal phases along with reflection spot resolution were used as a preliminary assessment of crystal quality.

2.2.3 Scanning Electron Microscopy and Energy Dispersive X-ray Spectrometry

Single crystal and powder samples are stuck to double-sided carbon tape that is attached to a carbon disk. The samples and disk are placed into a Hitachi S-3400N scanning electron microscope to obtain high resolution micrographs. This SEM has a beam energy of 30keV, thus ensuring we were seeing excitation associated with L and M shell- transitions in thorium and uranium. An Oxford INCO energy dispersive X-ray analysis detector captures characteristic X-rays simultaneously, providing elemental analysis. The elemental analysis is standardized using copper tape prior to sample identification.

2.2.4 Fluorescence Spectroscopy

Two types of fluorescence spectroscopy were used during this study: photoluminescence and cathodoluminescence. Photoluminescence (PL) relies on a material absorbing light of some wavelength by exciting an electron. This electron then undergoes de-excitation through non-radiative means via interaction with crystalline or molecular vibrational and rotational modes to a more stable excited state[28]. In a luminescent material the excited electron will relax back to the ground state through a radiative transition[28]. The light given off during this final transition

is detected as photoluminescence. PL provides high sensitivity information on trace impurity detection along with a measure of the band gap for a material[28]. Impurities we expect to find would include possible fluoride impurities along with silver impurities from the ampoules that the reactions take place in. Trace amounts of lanthanides and actinides may also be found because chemical separation is difficult, and commercially available thorium dioxide is 99.99% pure. We also plan to measure the band gap of our thorium dioxide single crystals. The band gap often quoted in the literature for thorium dioxide single crystals is 5.75 eV[29]. However, the band gap is expected to vary approximately linearly with dopant levels from Vegard's law[28]. Denton and Ashcroft offer this excellent definition of Vegard's law: "Vegard's law is an approximate empirical rule which holds that a *linear* relation exists, at constant temperature, between the crystal lattice constant of an alloy and the concentrations of the constituent elements." [30] Likewise, Vegard's law can describe the change in band gap energy with change in concentrations of constituent elements. This rule becomes very useful when engineering alloys to create a material with a desired band gap.

For photoluminescence, we used the Fluorolog -3 fluorspectrometer manufactured by the Horiba Scientific Corporation. The instrument works by passing light from a high voltage xenon lamp through a monochromator consisting of two sets of mirrors and two diffraction gratings. Two slits in the monochromator can be varied from 1 to 14nm to adjust the resolution of light passing through. The light incident on the sample will be reflected or absorbed and then emitted as fluorescent light. The reflected and emitted light passes through a similar monochromator before being passed to a photomultiplier tube. The wavelength settings and slit resolutions are both computer-controlled. The Fluorolog can run both excitation and emission experiments. In

excitation experiments, the emission monochromator is set to monitor a signal wavelength, while in emission experiments the excitation monochromator is set to provide a signal wavelength[31].

Cathodoluminescence is most simply defined as the emission of light as the result of electron beam bombardment[28]. This technique is ideally suited to gathering information on a material's electronic band structure and luminescence centers. For ThO_2 with a band gap approaching 6eV, CL circumvents the limited availability of optical sources able to excite across the band gap. The data gathered in this experiment consists of photons gathered by a cooled photomultiplier tube (PMT). These photons are in the ultraviolet, visible, and near-infrared regions of the spectrum and are generated by radiative relaxation between the conduction band, levels due to impurities and defects lying in the fundamental band gap, and the valence band[28]. Finally, we must consider that the electron is interacting with the solid via elastic and inelastic scattering processes, and that the depth of electron penetration is dependent on electron beam energy[28]. We can simulate this depth using software such as CASINO.

The specific instrument we used in our study employed an EMG-12 electron gun capable of beam energies between 100eV and 20keV and beam currents between 10nA and 100 μ A. The system was cooled to 20°C by a Leybold Coolpower 4.2 GM Crycooler, and a series of pumps evacuated the main chamber to pressures near 10^{-6} Torr. The fluorescence from the sample passes through a SPEX 500M monochromator with a spectral range of 1900-7000Å before being collected by a liquid nitrogen-cooled PMT. Finally, HORIBA's Scientific SynerJY software controls data acquisition and data analysis[32].

III. Crystal Growth and Characterization

3.1 Lowering the Synthesis Temperature of Bulk ThO₂

Lowering the synthesis temperature of ThO₂ single crystals offers two main advantages. First, lower synthesis temperatures subject the autoclaves and their constituent components to less thermal stress. This reduction in wear is likely to increase the lifetime of the equipment and the time between regular maintenance. Further, Mann's synthesis temperature of 750°C approached the highest safe operating temperature of the Inconel 718 Tuttle autoclaves. In this regard, lowering the synthesis temperature increases the likely scalability of the reaction while reducing the cost.

Secondly, intrinsic defect concentration is expected to exponentially increase with increasing temperature to a first approximation[33]. We can assume that the concentration of defects can be calculated from Boltzmann statistics and follows the formula:

$n_d \approx (N_T N^*)^{1/2} \exp(-\frac{\Delta H}{2kT})$, where n_d is the number of defects per unit volume, N_T is the number of total sites, N^* is the number of interstitial sites, ΔH is the defect formation enthalpy, k is Boltzmann's constant, and T is temperature. Calculating n_d for UO₂ at 670°C and 750°C with the following assumptions: neglect entropy because it will be similar for both cases, assume a Frenkel defect with an enthalpy of formation of 3.40eV[34] dominates, that there is 1 mole of UO₂, and that the interstitial is on the cation sublattice; we arrive at $n_{d,670^\circ C} = 2.01 \times 10^{13} cm^{-3}$ whereas $n_{d,750^\circ C} = 1.03 \times 10^{14} cm^{-3}$. We used UO₂ for the calculation because enthalpies of formation for intrinsic defects were readily available and UO₂ is structurally similar to ThO₂. This first order calculation demonstrates that changing the synthesis temperature by 80°C leads to a five-fold reduction in defect concentration.

To accomplish this decrease in synthesis temperature, the mineralizer concentration will have to be increased to compensate for the decreased solubility. As an example, at 9M CsF concentration the wt% solubility decreases by about 0.15wt% going from 750°C to ~670°C. Since ThO₂ already has low wt% solubility, this drop is a 27% decrease in wt% solubility, which is indicative of the amount of nutrient feedstock being brought into solution. The amount of feedstock in solution is directly related to the amount of material available for crystal growth. Hydrothermal solubility studies are a relative measure of solubility— solubility is most often measured in weight percent solubility (wt%), but this value does not pinpoint when a solution becomes saturated. Thus, weight percent solubility gives an idea of how soluble or insoluble a material is without a rigorous determination of the saturation point. Mann's prior work on the growth of bulk ThO₂ used 6M CsF to dissolve and transport the feedstock, and growth rates near 0.25mm/wk were shown. Using the solubility curves obtained by Mann and shown in Figure 10, we can estimate the mineralizer concentration needed for crystal synthesis at 670°C to be approximately between 0.32 - 0.40wt%. For this study, we chose to use 12M CsF because it likely has a comparable solubility of ThO₂ at 670°C as 6M CsF at 750°C. We expected to see comparable growth rates to Mann's synthesis because of the relatively similar solubility of the mineralizers.

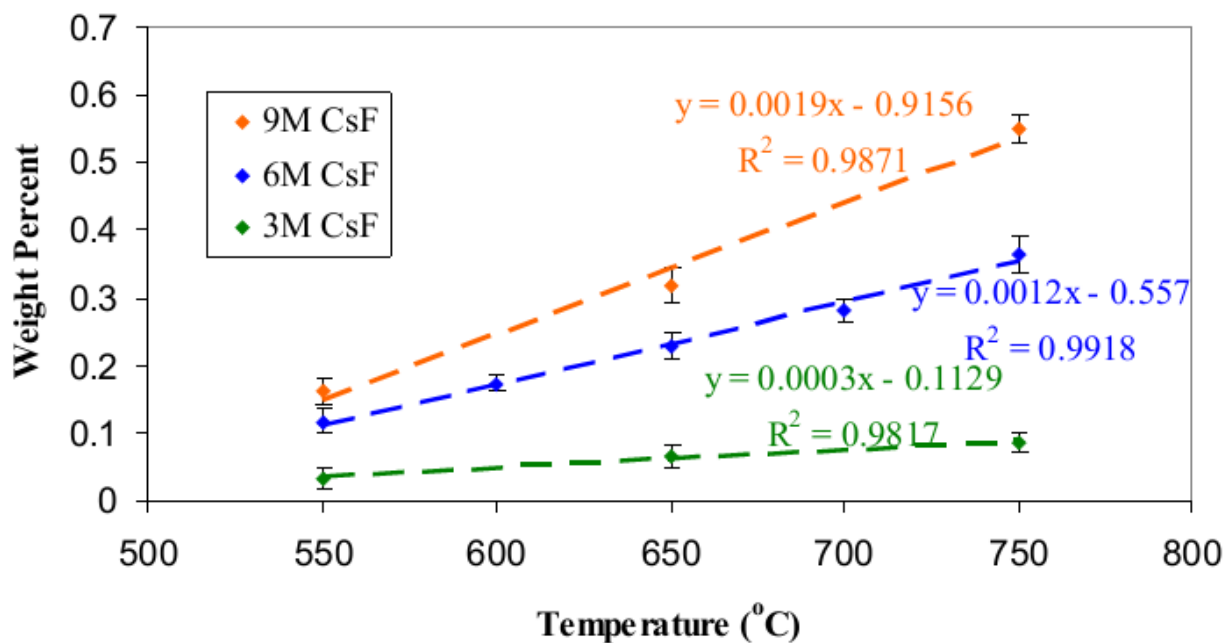


Figure 11. Solubility curves for ThO_2 at varying concentrations of CsF for three different temperatures: 550°C, 650°C, and 750°C. Using these solubility curves we can estimate the necessary CsF concentration for synthesis at 670°

The results of ThO_2 transport synthesis using 12M CsF is shown in Figure 11.

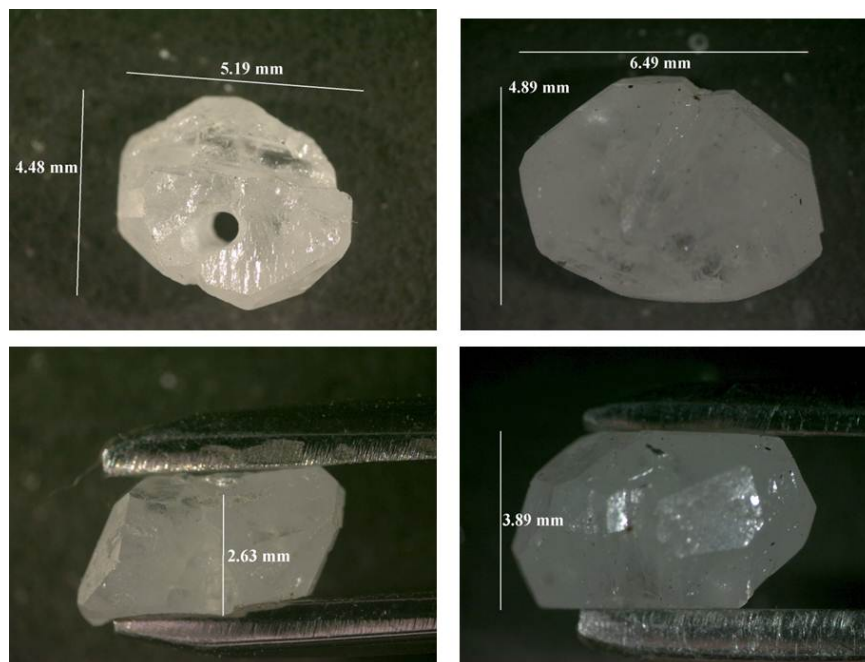


Figure 12. Bulk growth of ThO₂ using 12M CsF and a gradient of 670-635°C. The crystal grew 1mm in two dimensions in two months. The crystal is cloudy and irregularly shaped. The mineralizer concentration combined with the much lower synthesis temperatures likely resulted in a solution far too supersaturated and favorable to nucleation. These conditions likely contributed to the slower growth rates and low quality crystal growth. These results point to either using lower molarity or a shallower temperature gradient.

Growth rates were approximately 0.125mm/week in two dimensions. Since synthesis of ThO₂ at this temperature is a first, we cannot say whether higher growth rates are possible. Ideally, we would like to achieve growth rates approaching 0.25mm/wk in all dimensions. The lower growth rates likely resulted from spurious abundant nucleation happening inside the ampoule. An image of the nucleation next to the bulk crystal with a penny for scale is shown in Figure 12.



Figure 13. Comparison of nucleation produced during ThO_2 bulk growth using 12M CsF and a gradient of 670-635°C. The nucleation appeared to have come directly from the solution. Nucleation along the walls of the ampoules is often thin, rounded plates with small clusters of crystals. Characteristics of the reaction products guided future crystal synthesis experiments.

The amount of nucleation rivals the size of the bulk growth. Moreover, the nucleation does not have the shape of nucleation happening on silver walls suggesting it came out of solution. Excessive supersaturation from too large a gradient is likely to blame. In the solubility curves of Figure 10, there is a tendency for the slope of the curve to increase as the mineralizer is increased, which means we should reduce the gradient to reduce the solubility difference between the feedstock zone and the seed zone. In this study, the difference in solubility was too great, and ThO_2 crashed out of solution. The nucleation takes feedstock out of solution and away from the seed. Moreover, if there is some degree of solubility in the seed zone, the seed itself can be dissolved and transported onto nucleation sites further detracting from growth rates.

Additional evidence of an unfavorable mineralizer concentration and gradient combination is seen in the opaqueness of the bulk crystal. Opaqueness indicates defects within the crystal structure. With a band gap of 5.75eV, ThO_2 should be optically transparent. Also, Mann's crystal is less cloudy than the one shown in Figure 11, which is counterintuitive because Mann also had higher growth rates. Typically, slower growth rates correspond to higher quality

growth, but because of spurious nucleation from excessive supersaturation we saw poorer quality growth and slower growth rates. The upshot is that instantaneous growth rates may have been much larger than average growth rates. We report a growth rate for the entire duration of the growth, but the entire charge of feedstock could have been transported in a couple weeks – it is impossible to say for certain. Achieving high growth rates at the expense of quality could be beneficial when optical quality crystals are not needed.

We have demonstrated synthesis of ThO_2 at the lowest temperature to date, 670°C . We employed a higher mineralizer concentration than previous studies to compensate for the reduction in temperature. ThO_2 feedstock is clearly soluble and being transported to the seed zone, but the degree of supersaturation in the seed zone is too great. This is evidenced by the slow average growth rates, large amounts of nucleation, and poor quality growth seen on the seed. In future studies we will look to reduce the gradient and increase the temperature of the feedstock zone by a small amount.

3.2 Exploratory Growth of $\text{U}_x\text{Th}_{1-x}\text{O}_2$

Whether ThO_2 is to be used as a nuclear fuel or as a component of a neutron detection system it will need alloyed with uranium. Mann's previous work has shown successful growth of ThO_2 and lightly doped $\text{U}_x\text{Th}_{1-x}\text{O}_2$ with mole fraction values near 2-3%, but this work explores the growth of $\text{U}_x\text{Th}_{1-x}\text{O}_2$ with values of x ranging from 0.05 to 0.33.

As mentioned previously, before scaling the growth to larger and more time consuming reactions, we first looked at the reactions in smaller vessels producing smaller, microcrystalline powders. Microcrystalline powders tend to contain crystal with sizes in the micrometer range. Some of the reaction products are shown in Figure 13 below.



Figure 14. The microcrystalline powder obtained from crystal growth in 2.5" silver ampoules. This crystal growth focuses on the feasibility of alloying ThO_2 with U. From left to right the reactions were set up to produce ThO_2 , $\text{U}_{0.1}\text{Th}_{0.9}\text{O}_2$, $\text{U}_{0.5}\text{Th}_{0.5}\text{O}_2$, and UO_2 . However, using EDX, no uranium was found in the $\text{U}_{0.1}\text{Th}_{0.9}\text{O}_2$ reaction. Additionally, the $\text{U}_{0.5}\text{Th}_{0.5}\text{O}_2$ was measured to contain roughly 33% uranium, while the UO_2 is simply a UO_x compound. X-ray diffraction needs to be done to confirm the identity of the UO_x species.

Qualitatively, we expect a visible color change to darker olive tints to correspond with an increased mole fraction of the U^{4+} ion. Energy dispersive X-ray spectroscopy (EDX) was performed on all of the microcrystalline samples to assess the reaction products quantitatively. Scanning electron microscopy (SEM) was also performed to look at the morphology. The reactions were set up with temperatures of 670-630°C and in duplicate: one reaction used 6M CsF and the second one 12M CsF. The first reactions examined contained approximately 2% uranium in the reaction mix. SEM showed no difference in morphology of the crystals. EDX results for 2% uranium doping showed an absence of uranium. An EDX spectrum for the 2% uranium samples grown in 12M CsF is shown below in Figure 14.

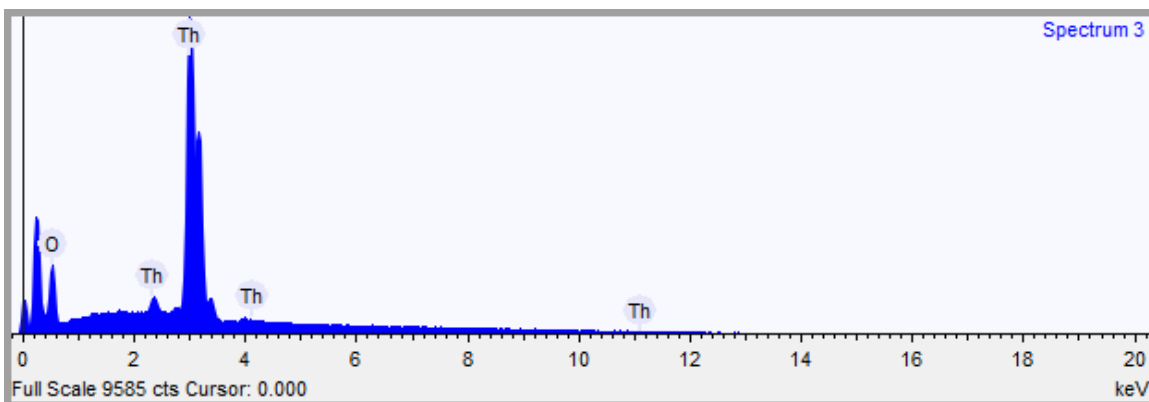


Figure 15. An EDX spectrum for a reaction with 2% uranium. There is no detectable uranium present in the sample. The accelerating voltage was 15keV and the acquisition time was 20s.

The second set of reactions contained 10% uranium. These reactions were also prepared in both 6M CsF and 12M CsF. SEM showed a marked difference in morphology between these reactions. The reaction containing 10% uranium and 6M CsF formed rod-like structures far different than the cubic structures expected. A SEM micrograph is shown in Figure 15.

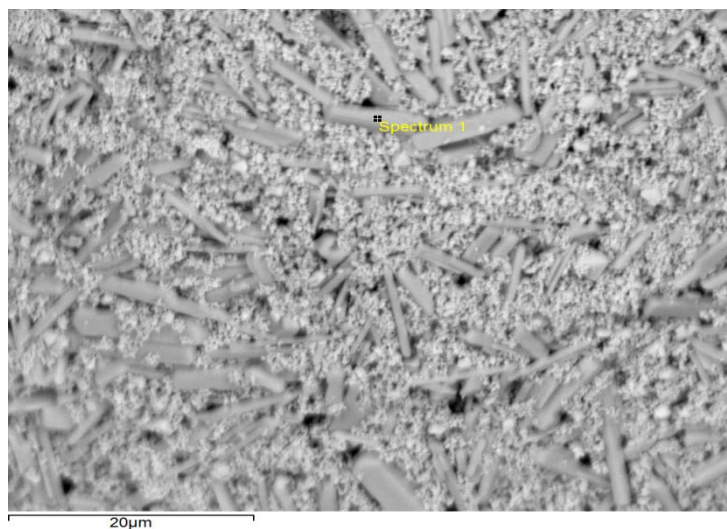


Figure 16. A micrograph of the small crystals produced from a reaction containing 10% uranium and 6M CsF. The rod-like structures are different from the expected cubic morphology – a good indication of an unwanted side product has formed.

Indeed, EDX results showed a product containing cesium, thorium, oxygen, and fluorine.

The EDX spectrum is shown below in Figure 16.

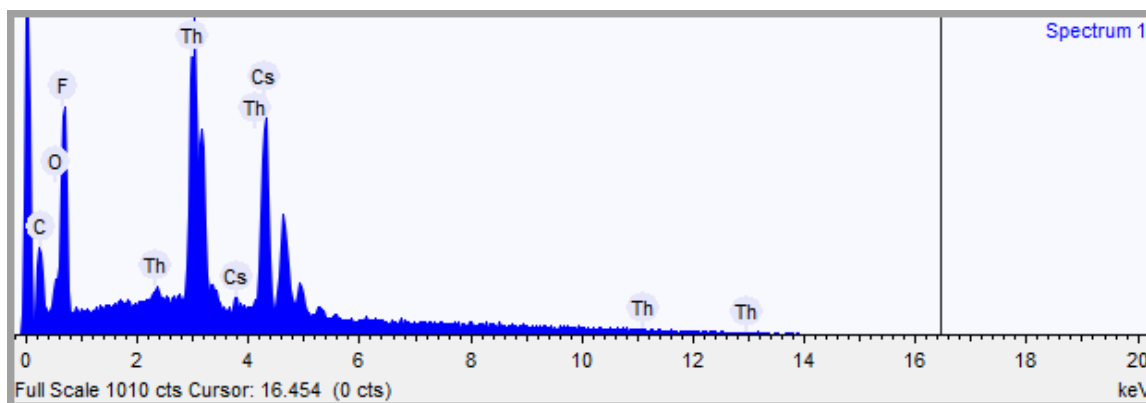


Figure 17. The EDX spectrum for the rod-like crystal structures produced. The peaks indicate the formation of a cesium, thorium, oxygen, and fluorine-containing side product.

In contrast, the 10% uranium and 12M CsF reaction showed the expected cubic morphology. However, the EDX spectrum again showed an absence of uranium. Qualitatively, though, the reaction product differs in color from the two feedstocks powders. The ThO_2 feedstock is white and the UO_2 feedstock is black. The reaction product contained the characteristic olive green tint associated with U^{4+} . Thus, the mole fraction of uranium present is likely below the instruments resolvable limit, roughly 1-2%. The results from the 2% experiment and the 10% experiment are first indications that a partition coefficient exists possibly because of the use of separate UO_2 and ThO_2 powders. A partition coefficient is a systematic difference between what the concentration should be versus what the actual value of the concentration of uranium. It is suspected that this partition coefficient is due to differences in solubility between ThO_2 and UO_2 in CsF. Specifically, we believe that UO_2 must have a lower solubility and a much smaller wt% of UO_2 is being solubilized, thus we see only a small fraction of uranium

present in the crystal. The results suggested the use of an alloyed feedstock, though at the time none were available.

For the next set of exploratory growth runs, the mole fraction of uranium included in the feedstock was increased to 50%. The morphology was in agreement with what was expected, and the EDX results showed the presence of uranium at a mole fraction of approximately 33%. The EDX spectrum is shown in Figure 17.

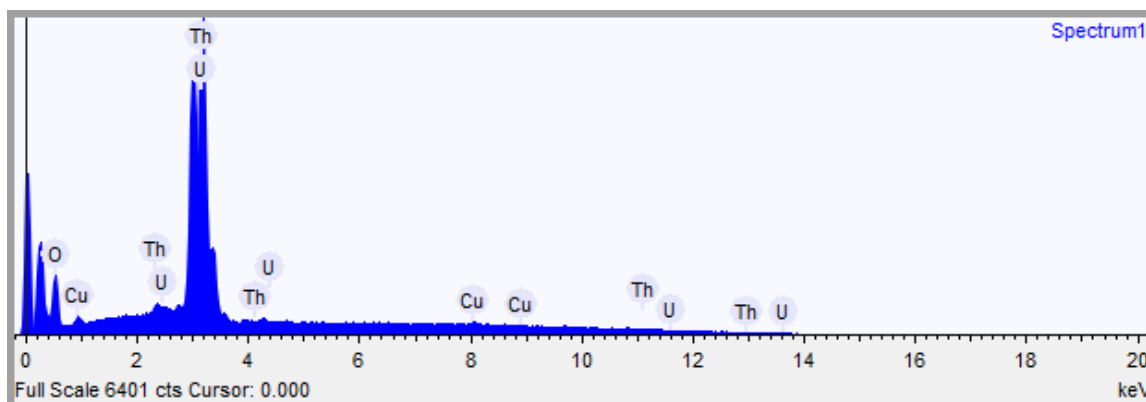


Figure 18. An EDX spectrum for a reaction with 50% uranium. There is approximately 33% uranium present in the sample. The accelerating voltage was 15keV and the acquisition time was 20s.

The final reaction performed in a small vessel contained only UO_2 and 12M CsF as mineralizer. The reaction product was analyzed using EDX and uranium to oxygen ratio was obtained that suggests a possible occurrence of UO_3 . However, EDX cannot be used to verify chemical identity and X-ray diffraction will have to be done to verify the chemical identity of the crystal. Additionally, EDX cannot detect hydrogen, and a hydrated uranium species is another possible candidate; hydrated species are quite common in hydrothermal solution. An SEM image is shown in Figure 18.

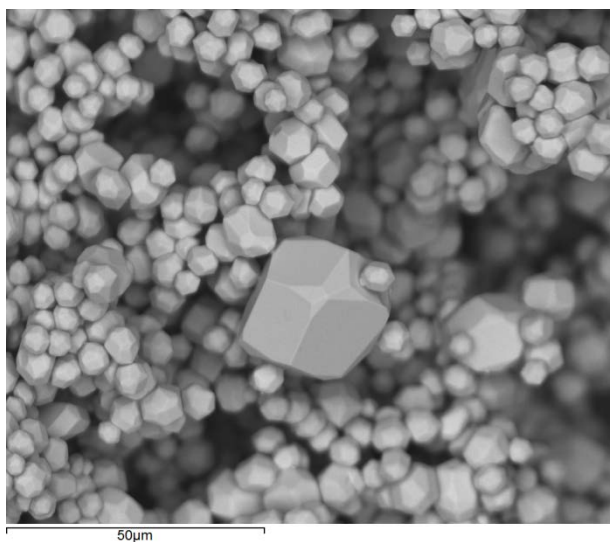


Figure 19. An electron micrograph of possible microcrystalline UO_3 . Powder or single crystal X-ray diffraction will have to be done to verify the chemical identity. The presence of major and minor faces is clearly visible. These micrographs are an indication of the success of the reaction in producing single crystals from mixed, powdered feedstock.

An EDX spectrum of the possible UO_3 species is shown in Figure 19.

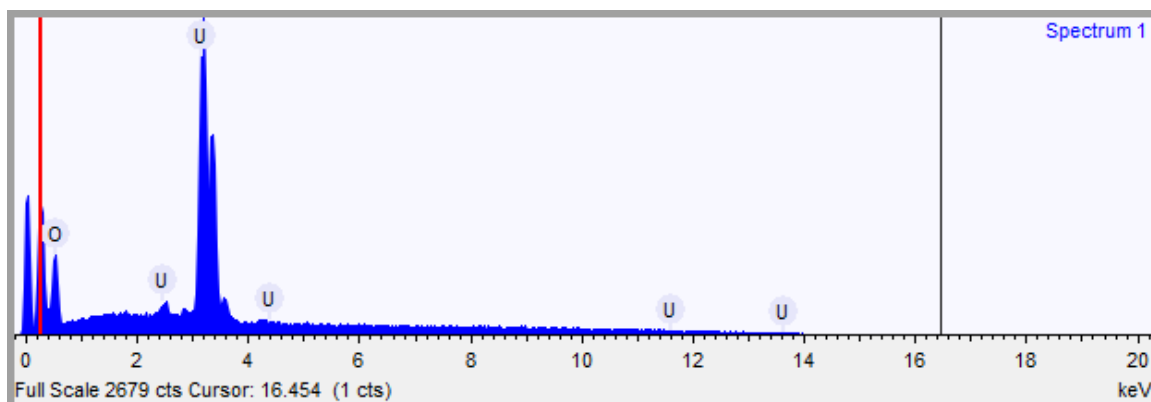


Figure 20. An EDX spectrum for a reaction containing only UO_2 and 12M CsF. The feedstock may have oxidized to UO_3 during crystallization. As stated above, X-ray diffraction will need to be done to determine the chemical identity. If uranium is found to be in the $6+$ oxidation state, the use of a templating agent like ThO_2 will be needed to stop the oxidation from U^{4+} to U^{6+} .

Qualitatively, we see a change in the color from the olive green associated with the U^{4+} to a deep red hue, possibly indicative of the U^{6+} state. This result portended the use of a templating seed to keep uranium in the 4+ oxidation state.

The exploratory growth in 2.5" ampoules and subsequent characterization signified the feasibility of growing bulk single crystals of $U_xTh_{1-x}O_2$. Specifically, the growth of microcrystalline powder with a mole fraction of roughly 33% uranium indicated the growth of bulk $U_xTh_{1-x}O_2$ with high doping levels likely.

3.3 Bulk Growth of $U_xTh_{1-x}O_2$

As mentioned prior, the exploratory growth runs were scaled up tenfold and a seed was used to encourage large growth in transport growth. The seed crystals were single crystal ThO_2 grown by Mann during his dissertation work. Given the matching crystal structures, relatively similar sizes of Th and U, and similar values of electronegativity; ThO_2 seeds were expected to work well in growing bulk $U_xTh_{1-x}O_2$. The use of ThO_2 seeds was also expected to act as a templating agent, an agent that would keep uranium in its 4+ oxidation state.

Two transport growths were set up. The first growth contained 20% UO_2 and 80% ThO_2 in the form of mixed powders. The second growth contained 40% UO_2 and 60% ThO_2 in the form of mixed powders. In both cases we increased the synthesis temperature to 685°C to increase the solubility of the reactants. The CsF mineralizer concentration was kept at 12M for both reactions, but the gradient for the 20% UO_2 reaction was reduced to 25°C gradient while the 40% UO_2 reaction had a 35°C gradient. By setting the reactions up with higher temperatures but different gradients, we could assess which condition led to higher quality growth and/or higher growth rates. However, both of these growths encountered technical difficulties.

The first growth run with 20% UO_2 is shown in Figure 20. New growth appears only on one side of the seed crystal suggesting that the ampoule may have collapsed and shielded one side of the seed from deposition. Additionally, we see a net loss of mass and hence a reduction in size in all dimensions.

Nucleation was still present as large plates forming along the ampoule walls and stand-alone single crystals. Rigorously comparing the amount of nucleation would have been difficult, yet given the resulting growth rates we can safely say the growth conditions were unfavorable for the growth of bulk $\text{U}_x\text{Th}_{1-x}\text{O}_2$.

Single crystal X-ray diffraction (SXRD) was performed on small pieces cleaved from the crystal. One piece was taken from the darker, thicker section while another was taken from the light section. The dark section had a lattice parameter of 5.5781(6) corresponding to a 13.7% uranium concentration by Vegard's law. The light sample had a lattice parameter of 5.5896(6) corresponding to a 4.7% uranium concentration by Vegard's law. While the crystal growth was beset with difficulties, the sample provided two lattice parameters to reinforce the idea that $\text{U}_x\text{Th}_{1-x}\text{O}_2$ alloys form a nearly ideal solid solution.

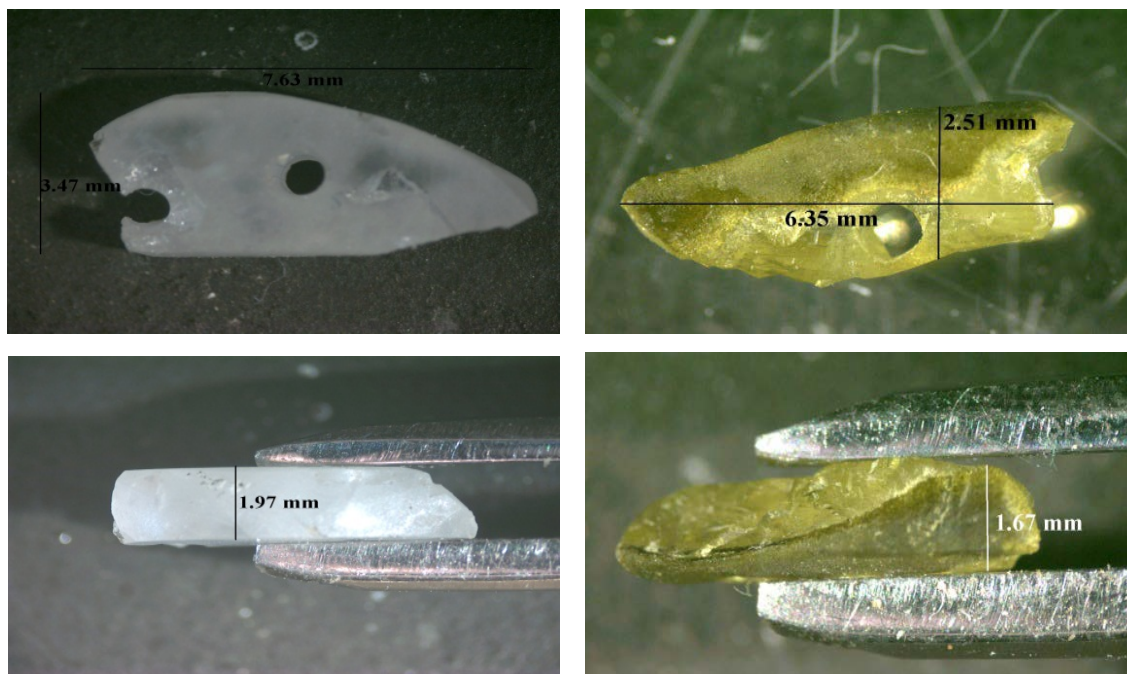


Figure 21. Bulk growth of $U_xTh_{1-x}O_2$ using 12M CsF and a gradient of 685-660°C. The crystal saw varied growth suggesting the ampoule crushed in around the crystal on one side. SXRD confirmed the sides had differing uranium concentrations.

A second reaction was run simultaneously, thus the conditions of this reaction were chosen without knowledge of the prior results. This reaction contained 40% UO_2 and 60% ThO_2 in the form of mixed powders. The results of the synthesis are shown Figure 21. The weld on the silver ampoule likely leaked for this reaction, thus the growth rates were slow. Growth rates were approximately 0.04mm/wk. When the weld broke was impossible to determine, so we cannot say how long this reaction was viable. Nonetheless, we visibly saw a layer of deep green new growth. Whether the opaqueness is a result of crystalline defects or a result of the Beer-Lambert law is difficult to say, though both factors are likely contributing.

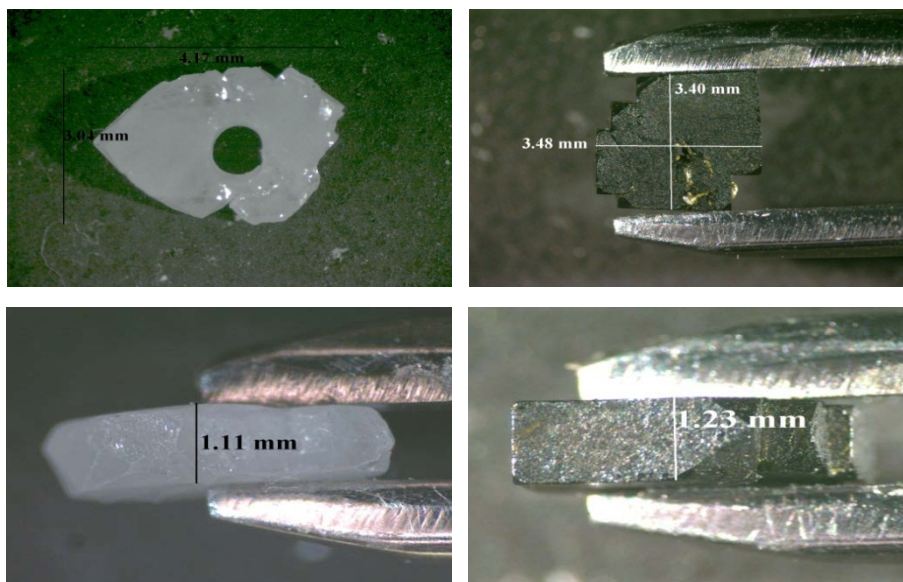


Figure 22. Bulk growth of $U_xTh_{1-x}O_2$ using 12M CsF and a gradient of 685-650°C. A uniform layer of uranium was deposited on the surface of the seed crystal. SXRD showed the uranium concentration to be 16%. Elemental mapping demonstrated that uranium appears to be spread homogenously throughout the crystal. The ampoule was lighter than usual suggesting the weld failed before the reaction was complete. Due to the black box nature of hydrothermal growth, it would be impossible to determine exactly when crystal synthesis stopped.

This reaction contained two distinct types of nucleation. One form of nucleation was a yellowish-green powder while the other was a black/very deep green crystal. The nucleation is imaged in Figure 22 for reference.

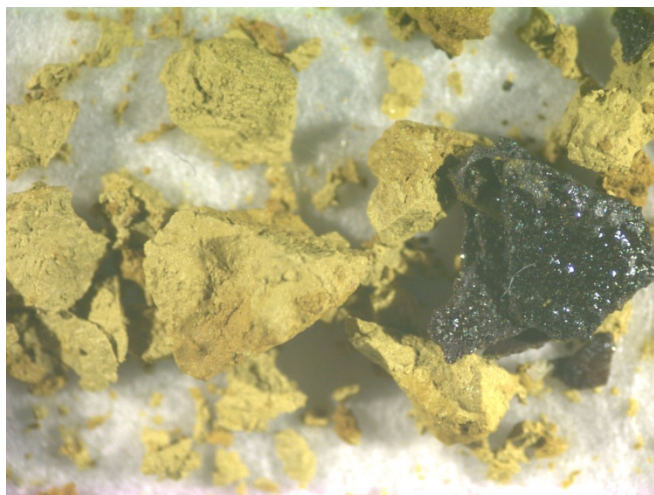


Figure 23. Nucleation from the reaction containing 40% uranium. At these high levels of uranium, side products of uranium oxides may be expected to form. Powder X-ray diffraction showed that each type of nucleation is an alloy of uranium and thorium, thus suggesting the ability of thorium to keep uranium in the +4 valence state.

With 40% uranium in the reaction mix it seemed plausible that the uranium was forming separate unwanted phases possibly in the U^{6+} valence state. Therefore, powder X-ray diffraction was performed on the two types of nucleation. The results showed that each type of nucleation was a thorium-uranium alloy with a different mole fraction of uranium. This result demonstrated that the thorium oxide was working to keep the uranium in the preferred U^{4+} oxidation state. The higher temperatures may have played a role, too.

Next, we wanted to verify that the uranium was incorporating homogeneously throughout the crystal. To answer this question, we used the Hitachi S-3400N scanning electron microscope to perform elemental mapping using energy dispersive X-ray spectroscopy. The results are shown in Figure 23.

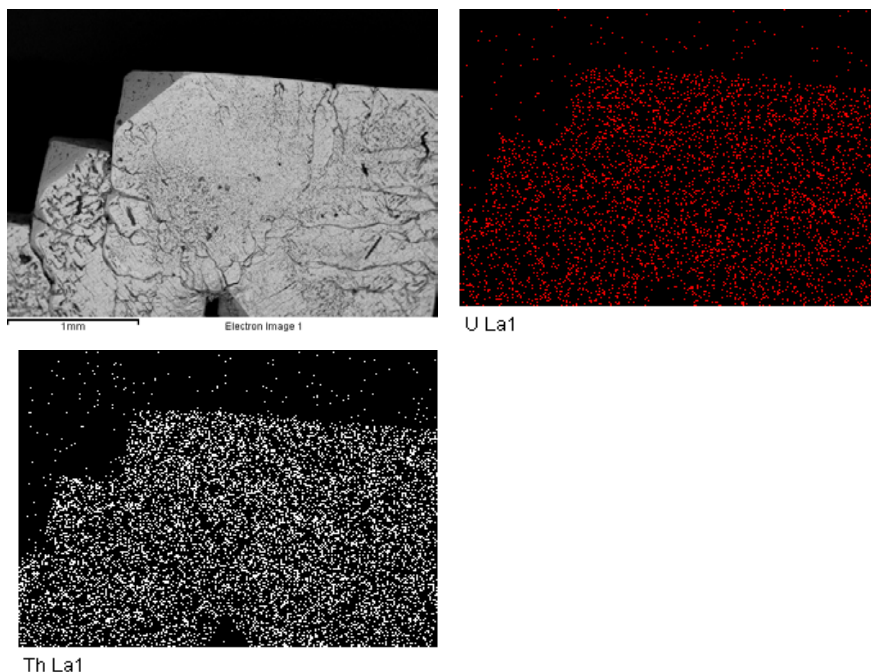


Figure 24. Elemental mapping of the bulk crystal with 16% uranium concentration. The beam energies were 30keV and easily able to induce L_{α} excitations. Qualitatively, the uranium distribution appears to be uniform.

Elemental mapping qualitatively suggested that the uranium was distributing evenly throughout the crystal. Homogenous distribution is further confirmed by plotting the lattice parameter against the thorium concentration.

Lastly, a small section of the crystal was removed using a wire saw. This small section was then cleaved into smaller pieces, and these pieces were mounted on glass fibers for single crystal X-ray diffraction. The lattice parameter obtained was $5.575(12)\text{\AA}$. The Laue patterns showed some pairs of reflections. The pairs could have resulted from twinning in the lattice or residual single crystal ThO_2 from the seed on the piece under investigation, though none was visible when using an optical microscope to mount the crystal.

These experiments produced the synthesis of $\text{U}_x\text{Th}_{1-x}\text{O}_2$ single crystals with mole fractions near 16%, 14%, and 5%. This study represents the first synthesis of $\text{U}_x\text{Th}_{1-x}\text{O}_2$ single

crystal with mole fractions of uranium greater than 4%. In our growths we also saw spurious nucleation, slow growth rates, and a difference between the concentration of UO_2 in the feedstock and the concentration of uranium in the single crystal. This difference was also observed in the exploratory growth runs. We believed these problems could be addressed by making three changes to the growth conditions. First, we needed to move to lower mineralizer concentration to reduce the solubility difference between the feedstock zone and the seed zone. Secondly, we would increase the synthesis temperature to 700°C and keep a 25°C gradient. This should increase the solubility of each zone while promoting sufficient mass transport of feedstock. Lastly, a pre-made, alloyed feedstock should be used to prevent low concentration of uranium in the final crystal. We suspected that UO_2 might be less soluble in CsF than ThO_2 leading to less UO_2 being in solution than expected. If we were to make $\text{U}_x\text{Th}_{1-x}\text{O}_2$ feedstock we would expect the mole fraction of uranium to match in the final crystal. These ideas were carried out in the final set of growth runs.

A final set of reactions with 20% uranium concentration and 40% uranium concentration were set up. The reaction containing 20% uranium differed from previous growth runs in three notable ways: the mineralizer molarity was lowered to 9M CsF , the temperature was raised to $700\text{-}675^\circ\text{C}$, and the feedstock was microcrystalline powder produced in a nucleation run. As mentioned previously, these changes were made to eliminate problems with spurious nucleation and differences in uranium concentration. The reaction containing 40% uranium also had a lower molarity of mineralizer and a higher reaction temperature, but the feedstock still consisted of mixed powders.

The reaction containing the nucleated feedstock showed growth rates likely near 0.2mm/wk , facets consisting of the major faces, and much smaller amounts of nucleation. The

crystal is shown in Figure 24. Due to the crystal's size and the available instrumentation, it would be impossible to get a lattice parameter on the crystal. However, an average of ten energy dispersive X-ray spectroscopy runs showed that the doping level is $23.1 \pm 0.7\%$, closely matching that of the nucleated powder used as feedstock.

The facets present on this crystal combined with the size make this crystal the best candidate to attempt a rocking curve measurement. Furthermore, this crystal will easily allow us to perform electron paramagnetic resonance (EPR) on an oriented sample, thus providing clues to the different types of impurities, crystal defects, and possibly uranium oxidation states.

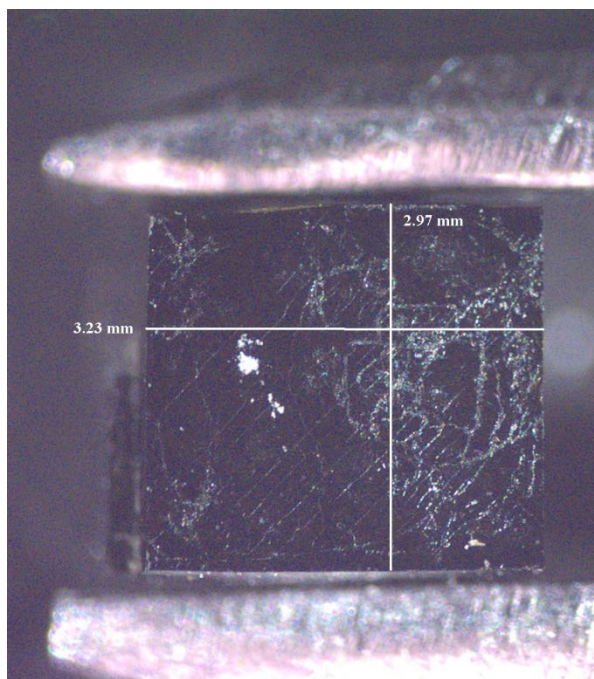


Figure 25. Bulk growth of a uranium-thorium alloy from a pre-fabricated feedstock. The temperature range was increased once more to 700-675°C while the mineralizer was brought down to 9M CsF. The result was approximately a cube 3mm on each side. The average of ten EDX results showed the doping level to be $23.1 \pm 0.7\%$.

The reaction containing the mixed powders with 40% uranium concentration produced a much different set of results. In this reaction, the seed was dissolved and fell off of the ladder.

Typically, this small amount of dissolution works to etch the surface free of impurities, however, in this case the dissolution was great enough to cause the seed crystal to fall off the ladder. A tell-tale sign of such an event is the intact silver wire used to hang the seed with loops where it had been tied around the seed crystal still present.

This implies that the seed crystal fell to the dissolution zone at the very beginning of the reaction because seed dissolution happens before the solution becomes saturated. Thus, the seed became feedstock, and the reaction became a nucleation run in a 7.5" silver ampoule. With that in mind, the reaction produced a large number of ~1mm crystals. Moreover, this reaction produced more and larger nucleation than a similar nucleation run using only mixed powders. EDX indicated the concentration of uranium to be between 25-31%. The nucleation from this run may serve to validate the results of the reaction employing pre-made feedstock.

These final growths of $U_xTh_{1-x}O_2$ were another first, pushing the concentration to 23% in the largest sample. Further, the growths demonstrated a good understanding of the growth process. Changes in the growth conditions produced crystals with growth rates likely approaching 0.2mm/wk, nearly five times previous growth rates for $U_xTh_{1-x}O_2$, and comparable to the synthesis of ThO_2 at 750°C. Further, the crystal is well faceted, which will lend itself to future characterization such as rocking curves and EPR. We encountered seed dissolution in the final growth, but the small ~1mm crystals produced can be used for feedstock to validate the results of the prior growth.

Finally, after discussing all the crystal growth, we can look at a plot of the lattice parameter against the concentration of thorium shown in Figure 25. The single large error bar at 84% thorium concentration is thought to result from poor preparation. The new growth was cut from the thorium seed using a wire saw. Some contamination from the wire saw or the seed may

have been on the crystal under investigation. The X-ray diffraction pattern sometimes contained additional spots. The linear result suggested that uranium-thorium oxide alloys form nearly ideal solid solutions and that the uranium is not clustering as it enters the lattice.

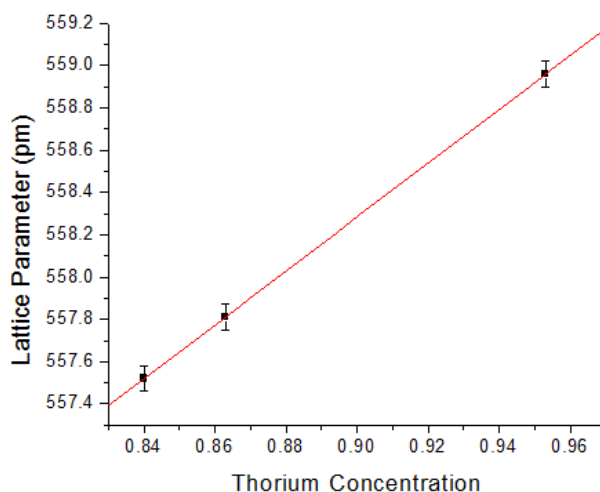


Figure 26. A plot of the lattice parameter against the concentration of thorium. This result shows that the alloys form a nearly ideal solid solution. The single large error bar at 84% thorium concentration is thought to result from poor preparation. The new growth was cut from the thorium seed using a wire saw. Some contamination from the wire saw or the seed may have been on the crystal under investigation. The X-ray diffraction pattern sometimes contained additional spots. However, the linear relationship tells us the uranium is distributing homogeneously and not clustering.

3.4 Structural and Optical Characterization of Spontaneous Nucleation

Single crystals of ThO_2 and $\text{U}_x\text{Th}_{1-x}\text{O}_2$ roughly ranging in size from 0.5mm to 3.0mm were used for structural and optical characterization. Structural characterization focused on understand defects and strain in the lattice, while optical characterization also studied defect formation while looking for material characteristics, specifically the band gap.

Mann has performed powder X-ray diffraction on similar crystals during the course of his thesis work as shown in Figure 6. Expanding on Mann's work, we obtained a rocking curve for

the urania-thoria alloy with roughly 23% uranium concentration to better understand how uranium incorporates into thoria single crystals and the resulting strain from such incorporation. With a rocking curve, the detector is fixed at a given angle (2θ), and the sample is “rocked” through a very small angular range (ω)[35]. One can estimate the dislocation density of a given sample by measuring the full width at half the maximum height (FWHM) of its rocking curve with the formula: $D = F^2/9b^2$, where D is the dislocation density, F is the FWHM in radians, and b is the Burger’s vector[35].

Performing a rocking curve requires having a well-faceted crystal. While we have not oriented the crystal under investigation due to its large size, we have evidence that the crystal faces do correspond to the atomic planes. Using SXRD, we verified that the cubic morphology corresponds to the expected crystallographic planes. Shown below in Figure 26 is an axial photograph of a small seed crystal. The crystallographic axes are displayed on the image in the center. Thus, we expect the faces of our cubic urania-thoria alloy correspond to the (100) planes.

The rocking curve for our alloy’s (200) plane is shown in Figure 27. From this data we can calculate the dislocation density to be $1.2 \times 10^9 \text{ cm}^{-2}$. Dislocation densities of annealed metals are typically between 10^6 - 10^8 cm^{-3} [36]. We expect using more pure starting materials and improving the reaction conditions will improve the dislocation density. Also, annealing would almost certainly decrease our dislocation density, but annealing would likely require temperatures near 2000°C, which is unfeasible.

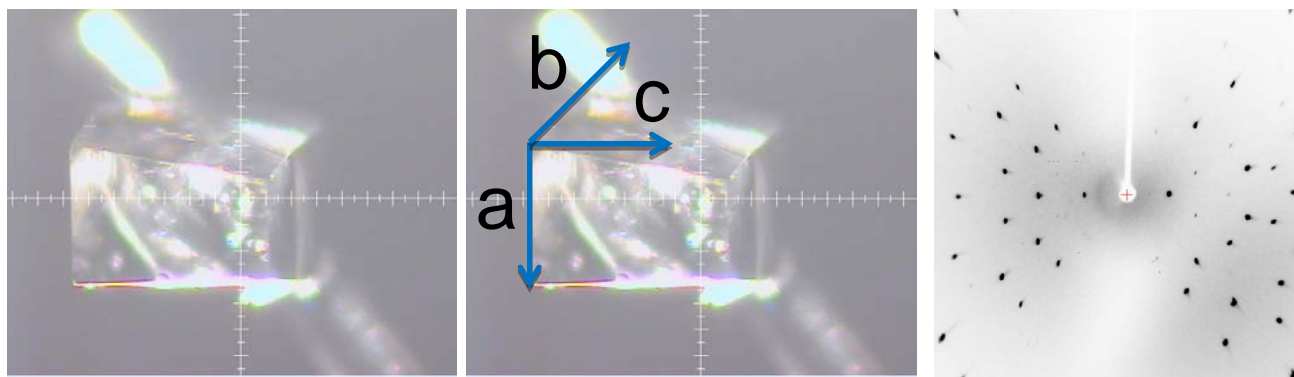


Figure 27. (Left) Axial photograph of a ThO_2 seed crystal as taken on the Rigaku AFC8 diffractometer. (Middle) The cubic crystal along with reference axes. To obtain these images four Laue patterns (Right) are collected and a crystal structure is input. Then, the software package calculates the amount of rotation needed to have the (100) face oriented perpendicular to the beam. As can be seen in the image, the flat faces of the crystal correspond to the (100) faces of the unit cell. (Right) A Laue pattern for the X-ray diffraction from the (100) plane. A symmetrical pattern with small, circular spots corresponds to the long-range order of single crystals.

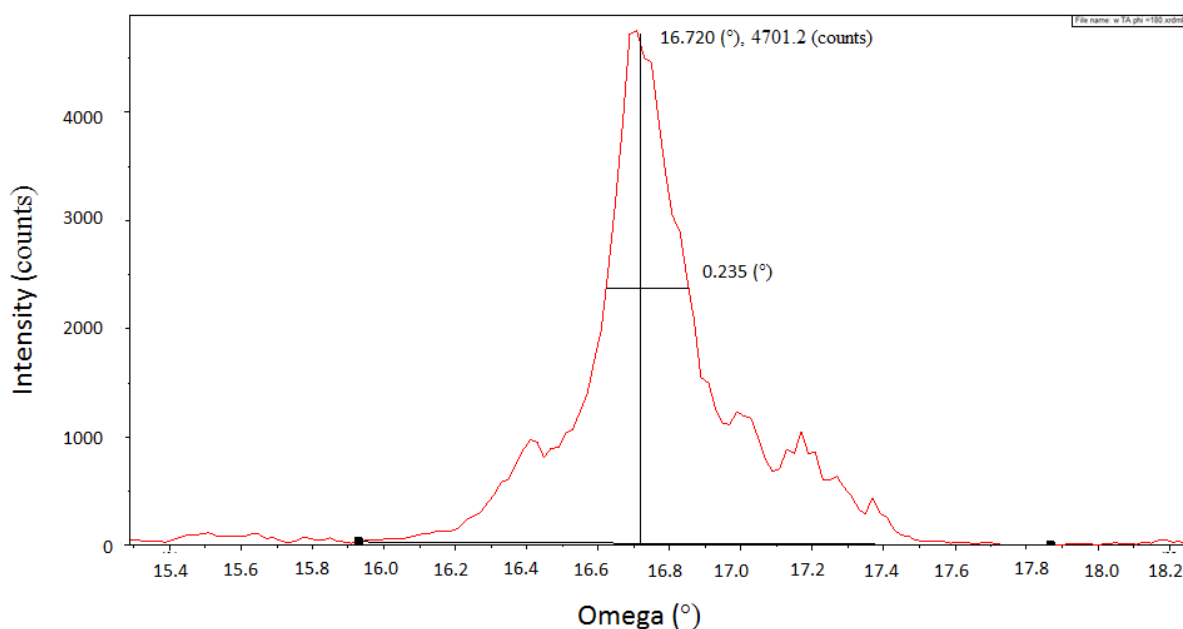


Figure 28. Rocking curve for the (200) plane in a urania-thoria alloy with roughly 23% uranium concentration. The FWHM of the rocking curve allows an approximate calculation of the dislocation density. We obtained a value of roughly $\sim 10^9$, whereas typical annealed metals are between 10^6 - 10^8 . We expect our dislocation density to improve with more pure starting materials and improved fabrication.

Preliminary investigation of thorium dioxide using PL yielded the following results shown in Figure 27.

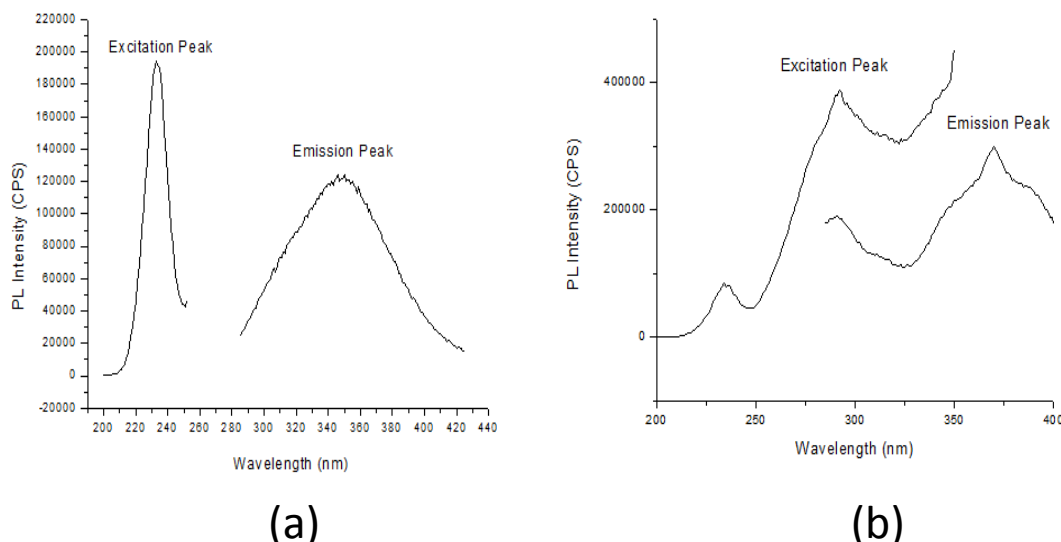


Figure 29. Photoluminescence spectrum for thorium dioxide. (a) We observe an excitation at 233nm light and an emission at 350nm light. (b) We observe an excitation at 291nm light and an emission at 371nm light.

We can only say a few things using just the PL spectrum. Since the shortest wavelength of light used to excite was 233nm, we are not able to excite at the energy of the band gap, which would require 215.6nm light. Therefore, we are most likely seeing transitions between acceptor levels and the conduction band or donor levels and the valence band. While we cannot identify the chemical species or quantity of the impurities, PL will be complementary to other techniques that can provide this information. The uranium-doped sample did not produce any signals.

The spontaneous nucleated crystals were subsequently investigated using cathodoluminescence (CL) spectroscopy. Before performing CL we should have an estimate for the depth of penetration of a given beam energy to ensure we are seeing effects from the bulk material and not just the surface. Simulating the depth of electron beam penetration can be done

using CASINO v2.4.8.1. CASINO is a Monte Carlo simulation of electron trajectory in solids.

The simulation of two thousand 20keV electrons striking ThO_2 is shown in Figure 29.

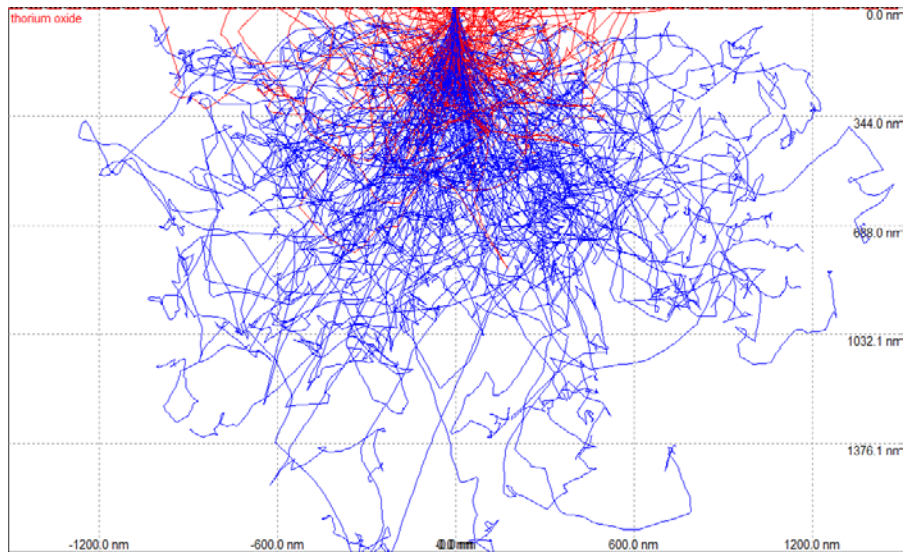


Figure 30. CASINO simulation of ThO_2 . The primary electrons (blue) appeared to penetrate to depths in excess of 1376.1nm. An approximation of the surface depth would be 100nm. This simulation ensured that the electrons would penetrate into the bulk sample.

We see that the primary electrons are interacting with the solid well past 300nm and thus interacting with the bulk solid. A rough approximation of the surface is 100nm of depth.

Similar results are obtained for the alloy $\text{U}_{0.04}\text{Th}_{0.96}\text{O}_2$ as shown in Figure 30

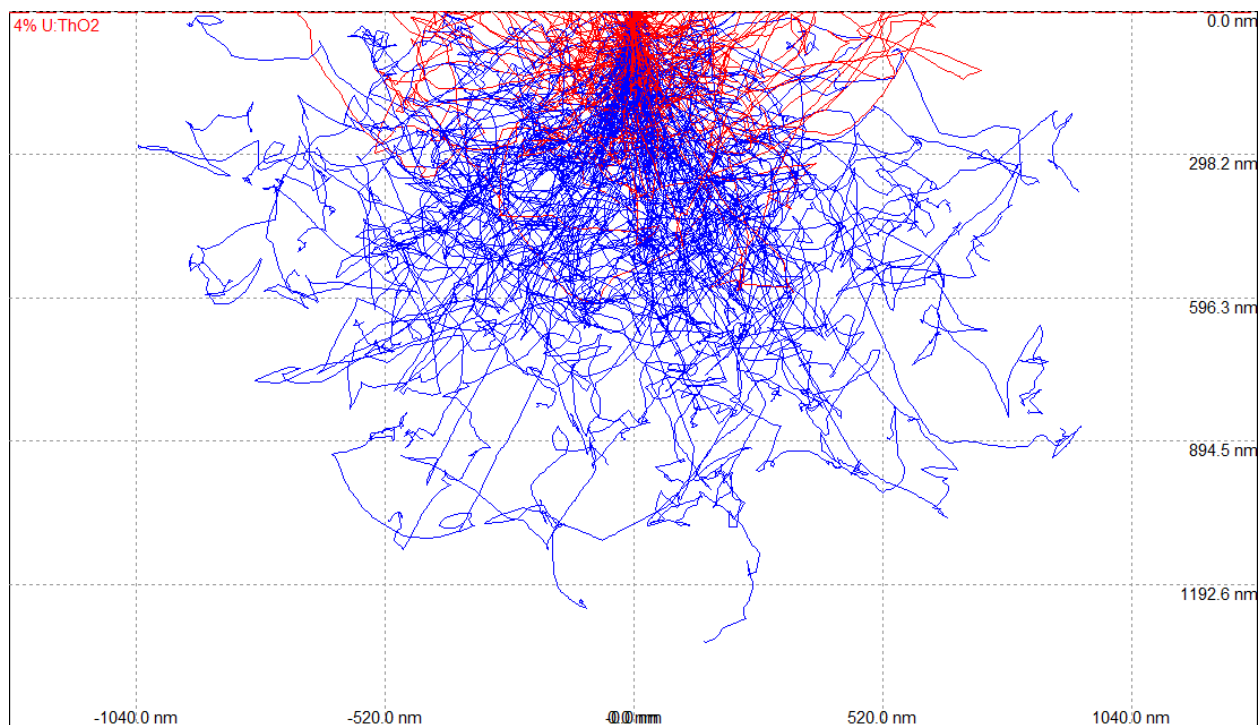


Figure 31. CASINO simulation $\text{U}_{0.04}\text{Th}_{0.96}\text{O}_2$. Like the ThO_2 sample, the simulation suggested we could probe beyond the surface because primary electrons are reaching depths near 900nm. Note, however, that the penetration depth is approximately 200nm less with 4% uranium because uranium has a larger nucleus.

Confident we would be probing the bulk crystal, we performed CL spectroscopy using a 20keV beam energy while having the sample cooled to ~25K. The PMT collecting the signal was also cooled to reduce noise. The sample gave off a bright blue/violet luminescence. The data collected for ThO_2 is shown in Figure 31.

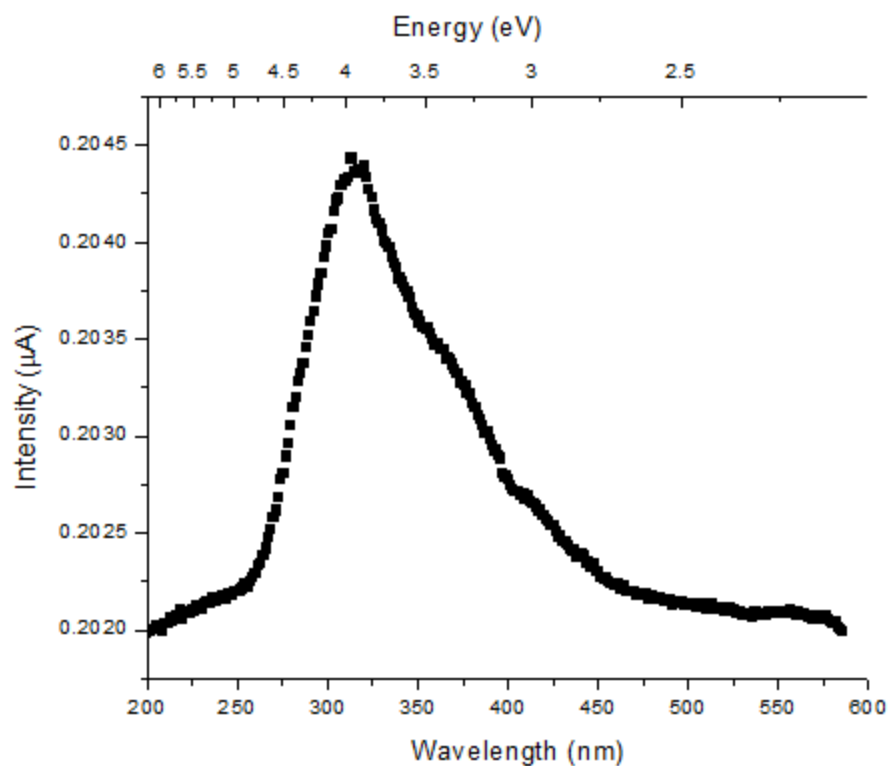


Figure 32. A ThO_2 spectrum collected using cathodoluminescence spectroscopy. The sample was cooled to 25K and bombarded with 20keV electrons. The sample emitted blue/violet light. The spectrum has four distinct features: the shoulder around 2300Å that keeps the main signal from going to baseline, the largest peak near 3300Å, then two remaining shoulders beyond the main peak. The peak around 3300Å closely matches the broad peak we saw using photoluminescence (PL). Likewise, a shoulder around 3700Å may be of the same origin as the 371nm peak seen using PL.

The signal obtained contained multiple shoulders. A preliminary fit of the signals was carried out using an interactive peak fitting program for Matlab created by Dr. O'Haver of the University of Maryland. The preliminary results are shown in Figure 32. The residuals demonstrate that the fit needs refinement, however the fit allows us to begin searching for candidate peaks in the literature. The peak positions were 235.7, 313.0, 365.5, 399.4, and 417.1nm. The broad peaks are indicative of impurities, possibly from solvent inclusions or crystalline defects.

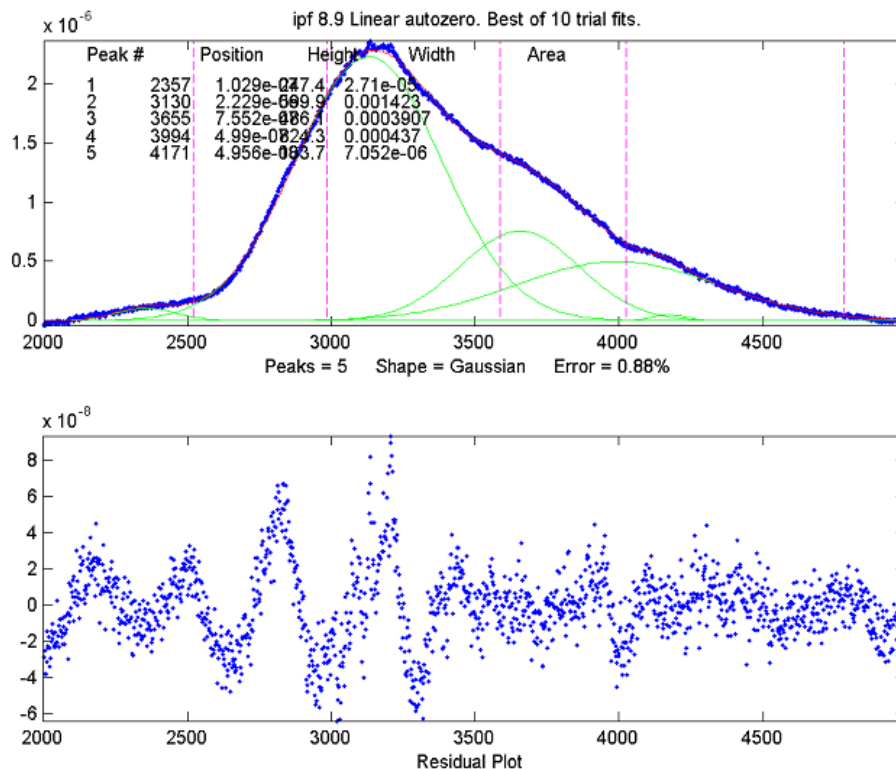


Figure 33. Preliminary CL fit for ThO₂ data. Using an interactive peak fitting program we fit five peaks to the spectrum and obtained an error of less than 1%. The peak positions were 235.7, 313.0, 365.5, 399.4, and 417.1nm. The peak positions gave a ballpark figure used to look for candidate peaks in the literature.

As mentioned previously, we also looked at a spontaneously nucleated U_xTh_{1-x}O₂ sample containing between 3-5% uranium. The data from that experiment is shown in Figure 33. The peaks are lower in intensity than in the ThO₂ sample. The rise beyond 7000Å is an artifact caused by the grating. Further runs with higher quality crystals should produce more intense peaks, though we used this spectrum to look for candidate peaks in the literature.

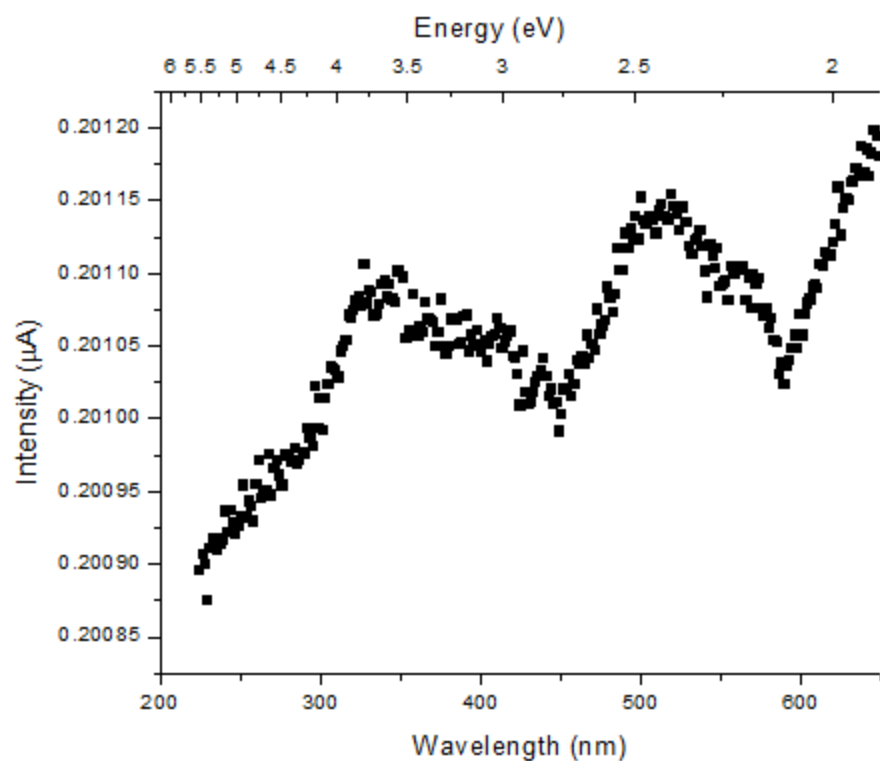


Figure 34. A $\text{U}_{0.04}\text{Th}_{0.96}\text{O}_2$ spectrum collected using cathodoluminescence spectroscopy. The sample was cooled to 25K and bombarded with 20keV electrons. The sample lacked any visible emissions. The peaks are weak in intensity and any shoulders cannot be discerned. However, the major peaks are a marked difference from results seen using PL. The peaks can be matched to peaks seen in the literature.

IV. Conclusions

4.1 Future Work

Relevant future work should include a solubility study of UO_2 . These solubility studies would enable an understanding of the difference in solubility between ThO_2 and UO_2 , while facilitating the synthesis of UO_2 . Obtaining more pure uranium and growing UO_2 in bulk is a future aim of this research.

More in-depth characterization of the structural and optical properties $\text{U}_x\text{Th}_{1-x}\text{O}_2$ would provide a better understanding of the physical changes that occur in these materials. Characterization could include thermal measurements, measurements of band structure, and secondary ion mass spectrometry to establish what impurities and phases reside in the crystal structure. All such characterization would represent a baseline pertaining to the first synthesis of these materials.

Lastly, modeling the conditions inside the autoclave would impart a better understanding of the chemistry and physics happening inside the autoclave. An improved understanding could lead to a much improved and more efficient crystal growth method.

4.2 Conclusions

Fabrication of uranium-thorium oxide alloys using pressed ceramics has been studied extensively for years. Developing next generation, thorium breeding nuclear fuel motivates much of this research. However, single crystals are expected to exhibit or have exhibited chemical properties more favorable to this aim. These properties include improved thermal conductivity and better chemical stability. Moreover, single crystals possess a far wider range of applications

including lasers and semiconductor devices. The extremely refractory nature of thorium oxide has stalled single crystal synthesis using more traditional melt and flux techniques. Large single crystal thorium oxide was finally synthesized by Mann during his investigations of hydrothermal growth of tetravalent oxide compounds.

This research looked to optimize the crystal growth of thorium oxide and eventually grow uranium-thorium oxide alloys. We sought to increase the concentration of the mineralizer to compensate for lower synthesis temperatures while maintaining similar growth rates for thorium oxide. Lower temperatures were expected to improve the scalability of the reaction, decrease the number of intrinsic defects, and reduce wear and tear on the experimental apparatuses. The resulting crystal growth suffered from poor quality and abundant parasitic growth. The high mineralizer concentration combined with a 35°C gradient likely led to an excessive degree of supersaturation. Future growth experiments may seek to synthesize ThO_2 at similar temperatures but with a lower mineralizer concentration or smaller gradient.

We then decided that growth of $\text{U}_x\text{Th}_{1-x}\text{O}_2$ single crystals more closely matched the motivations of the research. The crystal growth conditions from ThO_2 were likely to translate well to growth of $\text{U}_x\text{Th}_{1-x}\text{O}_2$ crystals. Exploratory growth in 2.5” silver ampoules confirmed expectations. Uranium-thorium alloys were produced with uranium concentrations near 33%. Though EDX data was inconclusive for samples set up with less than 10% uranium, powder color indicated the presence of uranium. The presence of a partition coefficient would be a recurring theme in crystal growth relying on mixed powder. EDX data did show the presence of uranium in a reaction set up with a 50/50 mix of thorium oxide and uranium oxide powders. Only one side product was seen, which was never reproduced in later experiments. Lastly, when

thorium oxide was not included in the reaction, a possible uranyl oxide was produced thus suggesting the presence of thorium was keeping uranium from oxidizing to the +6 valence state.

Four seeded synthesis experiments were performed. Each growth produced better results as conditions were optimized. The first set of experiments were with 20% uranium concentration and 40% uranium concentration, a gradient of 685-660°C and 685-650°C, respectively, and both had a mineralizer concentration of 12M CsF. Both synthesis experiments experienced technical difficulties, but the experiments demonstrated the feasibility of growing $U_xTh_{1-x}O_2$ crystals with values of the mole fraction being greater than 10%. Notably, the 40% uranium alloy had an even layer of growth, facets, and an actual concentration of 16% uranium. The partition coefficient witnessed in exploratory growth was also present. Mixed powders of 40% uranium oxide and 60% thorium oxide produced crystals containing 16% uranium. This partition coefficient disappears when using a pre-made feedstock; this will be discussed further below. Large amounts of parasitic growth were still present suggesting we should dial back the mineralizer concentration—too high a degree of supersaturation was still a problem. SXRD data shows errors on the order of 0.01%, indicating a very well structured crystal.

Lastly, we grew a faceted crystal with significant new growth and less parasitic growth when using a pre-fabricated feedstock. The doping level between the feedstock and the crystal also matched when using a pre-fabricated feedstock. When using mixed powders, we often see less than half of the expected doping. We have also shown a difference in nucleation as the temperature is raised and the concentration of mineralizer is lowered. These differences in temperature are relatively small, a difference of 15°C with temperatures near 700°C. The mineralizer concentration is also a relatively small change: decreasing from 12M to 9M CsF. Yet, we saw a noticeable difference in the amount of parasitic growth.

Overall, the growth of bulk $U_xTh_{1-x}O_2$ crystals with mole fractions of ~23% has been demonstrated. Reaction conditions for this growth have been optimized and suitable substrate material has been chosen. This research offers a way of looking into next generation nuclear fuels along with possibly offering a new way to look at waste disposal of spent fuel. Additionally, these growths are a step towards a metal oxide semiconductor employing uranium and thorium.

Bibliography

- [1] B. K. Sovacool, "Valuing the greenhouse gas emissions from nuclear power: A critical survey," *Energy Policy*, vol. 36, no. 8, pp. 2950–2963, Aug. 2008.
- [2] *Thorium Fuel Cycle - Potential Benefits and Challenges*. International Atomic Energy Agency, 2005.
- [3] G. Rayner-Canham and T. Overton, *Descriptive Inorganic Chemistry, Third Edition*. W. H. Freeman, 2002, p. 569.
- [4] S.-Y. Wu and H.-N. Dong, "Studies on the local structure and the g factors for the tetragonal Er^{3+} center in ThO_2 ," *Journal of Alloys and Compounds*, vol. 451, no. 1–2, pp. 248–250, Feb. 2008.
- [5] S. L. Chaplot, R. Mittal, and N. Choudhury, Eds., *Thermodynamic Properties of Solids: Experiments and Modeling*. John Wiley & Sons, 2010, p. 342.
- [6] K. Bakker, E. H. P. Cordfunke, R. J. M. Konings, and R. P. C. Schram, "Critical evaluation of the thermal properties of ThO_2 and $\text{Th}_{1-y}\text{U}_y\text{O}_2$ and a survey of the literature data on $\text{Th}_{1-y}\text{Pu}_y\text{O}_2$," *Journal of Nuclear Materials*, vol. 250, no. 1, pp. 1–12, Nov. 1997.
- [7] C. G. S. Pillai and P. Raj, "Thermal conductivity of ThO_2 and $\text{Th}_{0.98}\text{U}_{0.02}\text{O}_2$," *Journal of Nuclear Materials*, vol. 277, no. 1, pp. 116–119, Jan. 2000.
- [8] J. Stultz, M. T. Paffett, and S. A. Joyce, "Thermal Evolution of Hydrogen Following Water Adsorption on Defective UO_2 (100)," *The Journal of Physical Chemistry B*, vol. 108, no. 7, pp. 2362–2364, Feb. 2004.
- [9] J. M. Haschke, "Thermodynamics of water sorption on PuO_2 : Consequences for oxide storage and solubility," *Journal of Nuclear Materials*, vol. 344, no. 1–3, pp. 8–12, Sep. 2005.
- [10] M. Mann, D. Thompson, K. Serivalsatit, T. M. Tritt, J. Ballato, and J. Kolis, "Hydrothermal Growth and Thermal Property Characterization of ThO_2 Single Crystals," *Crystal Growth & Design*, vol. 10, no. 5, pp. 2146–2151, May 2010.
- [11] C. Ronchi and J. P. Hiernaut, "Experimental measurement of pre-melting and melting of thorium dioxide," *Journal of Alloys and Compounds*, vol. 240, no. 1–2, pp. 179–185, 1996.

- [12] J. . Keem, H. R. Harrison, S. P. Faile, H. Sato, and J. M. Honig, "No Title," *American Ceramic Society Bulletin*, no. 56, p. 1022, 1977.
- [13] C. C. Herrick and R. G. Behrens, "Synthesis of refractory-oxide materials by skull melting," *Journal of Crystal Growth*, no. 51, pp. 183–189, 1981.
- [14] T. S. Laszlo, P. J. Sheehan, and R. E. Gannon, "Thoria single crystals grown by vapor deposition in a solar furnace," *Journal of Physics and Chemistry of Solids*, vol. 28, no. 2, pp. 313–316, Feb. 1967.
- [15] R. C. Linares, "No Title," *J. Phys. Chem. Solids*, no. 28, pp. 1285–1291, 1967.
- [16] B. M. Wanklyn and B. J. Garrard, "The flux growth of large thoria and ceria crystals," *Journal of Crystal Growth*, vol. 66, no. 2, pp. 346–350, Mar. 1984.
- [17] C. B. Finch and G. W. Clark, "Single-Crystal Growth of Thorium Dioxide from Lithium Ditungstate Solvent," *Journal of Applied Physics*, vol. 36, no. 7, p. 2143, Jul. 1965.
- [18] A. B. Chase and J. A. Osmer, "No Title," *American Mineralogist*, no. 49, pp. 1469–1471, 1964.
- [19] J. M. Mann, "HYDROTHERMAL CRYSTAL GROWTH OF TETRAVALENT AND PENTAVALENT METAL OXIDES," Clemson University, 2009.
- [20] A. A. Ballman and R. A. Laudise, "Hydrothermal Growth," in *The Art and Science of Growing Crystals*, 1963, pp. 231–251.
- [21] "Supercritical Fluid." [Online]. Available: <http://www.springerreference.com/docs/html/chapterdbid/325520.html>. [Accessed: 08-Feb-2013].
- [22] E. Kiran, P. G. Debenedetti, and C. J. Peters, Eds., *Supercritical Fluids: Fundamentals for Application (Google eBook)*. Springer, 1994, p. 820.
- [23] K. Byrappa, *HANDBOOK OF HYDROTHERMAL TECHNOLOGY*. Noyes Publication, 2001.
- [24] C. McMillen and J. Kolis, "Bulk single crystal growth from hydrothermal solutions," *Philosophical Magazine*, no. June, pp. 37–41, 2012.
- [25] R. J. D. Tilley, *Understanding Solids: The Science of Materials (Google eBook)*. John Wiley & Sons, 2005, p. 616.
- [26] Y. Leng, *Materials Characterization: Introduction to Microscopic and Spectroscopic Methods*. John Wiley & Sons, 2008, p. 337.

- [27] O. F. Tuttle, "A New Hydrothermal Quenching Apparatus," *Amer. J. Sci.*, vol. 246, pp. 628–635, 1948.
- [28] C. R. Brundle, C. A. Evans, and S. Wilson, *Encyclopedia of Materials Characterization: Surfaces, Interfaces, Thin Films*. Gulf Professional Publishing, 1992, p. 751.
- [29] E. Rodine and P. Land, "Electronic Defect Structure of Single-Crystal ThO₂ by Thermoluminescence," *Physical Review B*, vol. 4, no. 8, pp. 2701–2724, Oct. 1971.
- [30] A. Denton and N. Ashcroft, "Vegard's law," *Physical Review A*, vol. 43, no. 6, pp. 3161–3164, Mar. 1991.
- [31] D. A. Buchanan, "EPR AND ENDOR STUDIES OF POINT DEFECTS IN LITHIUM TETRABORATE," Air Force Institute of Technology, 2012.
- [32] M. Lee, "Cathodoluminescence of Refractory Oxides," Air Force Institute of Technology, 2012.
- [33] M. . Barsoum, *Fundamentals of Ceramics (Google eBook)*, vol. 2002. CRC Press, 2002, p. 624.
- [34] L. Smart and E. A. Moore, *Solid State Chemistry: An Introduction, 2nd Edition*. CRC Press LLC, 1995, p. 379.
- [35] S. A. Speakman, "Introduction to High Resolution X-Ray Diffraction of Epitaxial Thin Films." [Online]. Available: [http://prism.mit.edu/xray/Introduction to HRXRD.pdf](http://prism.mit.edu/xray/Introduction%20to%20HRXRD.pdf).
- [36] B. K. Agrawal, *Introduction to Engineering Materials*. Tata McGraw-Hill Education, 1988, p. 353.

REPORT DOCUMENTATION PAGE			Form Approved OMB No. 0704-0188	
<p>The public reporting burden for this collection of information is estimated to average 1 hour per response, including the time for reviewing instructions, searching existing data sources, gathering and maintaining the data needed, and completing and reviewing the collection of information. Send comments regarding this burden estimate or any other aspect of this collection of information, including suggestions for reducing this burden to Department of Defense, Washington Headquarters Services, Directorate for Information Operations and Reports (0704-0188), 1215 Jefferson Davis Highway, Suite 1204, Arlington, VA 22202-4302. Respondents should be aware that notwithstanding any other provision of law, no person shall be subject to any penalty for failing to comply with a collection of information if it does not display a currently valid OMB control number. PLEASE DO NOT RETURN YOUR FORM TO THE ABOVE ADDRESS.</p>				
1. REPORT DATE (DD-MM-YYYY) 21-03-2013		2. REPORT TYPE Master's Thesis		3. DATES COVERED (From — To) Jun 2012 – December 2012
4. TITLE AND SUBTITLE Crystal Growth and Characterization of ThO ₂ and U _x Th _{1-x} O ₂		5a. CONTRACT NUMBER		
		5b. GRANT NUMBER		
		5c. PROGRAM ELEMENT NUMBER		
6. AUTHOR(S) Castilow, Jacob G.		5d. PROJECT NUMBER		
		5e. TASK NUMBER		
		5f. WORK UNIT NUMBER		
7. PERFORMING ORGANIZATION NAME(S) AND ADDRESS(ES) Air Force Institute of Technology Graduate School of Engineering and Management (AFIT/ENY) 2950 Hobson Way WPAFB OH 45433-7765		8. PERFORMING ORGANIZATION REPORT NUMBER AFIT-ENP-13-M-06		
9. SPONSORING / MONITORING AGENCY NAME(S) AND ADDRESS(ES) Heather Nickle Oak Ridge Institute for Science and Education 4692 Millennium Drive Suite 101 Belcamp, MD 21017 United States		10. SPONSOR/MONITOR'S ACRONYM(S) ORISE		
		11. SPONSOR/MONITOR'S REPORT NUMBER(S)		
12. DISTRIBUTION / AVAILABILITY STATEMENT APPROVED FOR PUBLIC RELEASE; DISTRIBUTION UNLIMITED				
13. SUPPLEMENTARY NOTES This material is declared a work of the U.S. Government and is not subject to copyright protection in the United States.				
14. ABSTRACT <p>Hydrothermal synthesis of ThO₂ and U_xTh_{1-x}O₂, and UO_x at temperatures between 670°C and 700°C has been demonstrated. Synthesis at these temperatures is 50-80°C below prior crystal growths and represents a new lower bound of successful growth. Hydrothermal synthesis represents a cost effective, environmentally friendly way of growing bulk actinide materials of optical quality. These refractory oxide single crystals offer potential applications in thorium nuclear fuel technology, wide-band-gap uranium-based direct-conversion solid state neutron detectors, and understanding how actinide fuels age with time. ThO₂ single crystals of dimensions 6.49mm x 4.89mm x 3.89 mm and weighing 0.633g have been synthesized at growth rates near 0.125mm/wk. Single crystal U_xTh_{1-x}O₂ crystals with mole fractions up to x≈0.30 have also been grown. The largest alloyed crystal with mole fraction x ≈0.23 has dimensions of 2.97mm x 3.23mm x ~3mm and saw growth rates likely near 0.2mm/wk. Mineralizer molarity, temperature gradient, and synthesis temperature were gradually optimized to produce a faceted, cubic crystal approximately 3mm a side. X-ray diffraction of single crystal ThO₂ determined the unit cell to be of the calcium fluorite structure with a lattice parameter of 5.596(4)Å. Lattice parameters for U_xTh_{1-x}O₂ varied linearly with thorium concentration suggesting homogenous uranium incorporation into the lattice.</p>				
15. SUBJECT TERMS hydrothermal thorium uranium actinide oxide				
16. SECURITY CLASSIFICATION OF:		17. LIMITATION OF ABSTRACT	18. NUMBER OF PAGES	19a. NAME OF RESPONSIBLE PERSON
a. REPORT	b. ABSTRACT			c. THIS PAGE
U	U	UU	72	19b. TELEPHONE NUMBER (Include Area Code) (937)255-3636, ext 4695; timothy.zens@afit.edu